

### RESEARCH ARTICLE OPEN ACCESS

# Altered Primary Somatosensory Neuron Development in a *Pten* Heterozygous Model for Autism Spectrum Disorder

Alejandra Fernandez<sup>1</sup> | Nick Sarn<sup>2</sup> | Charis Eng<sup>2,3,4</sup> | Kevin M. Wright<sup>1</sup>

<sup>1</sup>Vollum Institute, Oregon Health & Science University, Portland, Oregon, USA | <sup>2</sup>Genomic Medicine Institute, Lerner Research Institute, Cleveland Clinic, Cleveland, Ohio, USA | <sup>3</sup>Center for Personalized Genetic Healthcare, Medical Specialties Institute, Cleveland Clinic, Cleveland, Ohio, USA | <sup>4</sup>Department of Genetics and Genome Sciences, Case Western Reserve University School of Medicine, Cleveland, Ohio, USA

Correspondence: Alejandra Fernandez (alejandra.fernandez @utrgv.edu) | Kevin M. Wright (wrighke@ohsu.edu)

Received: 3 February 2025 | Revised: 18 August 2025 | Accepted: 28 August 2025

Funding: This work was supported by the National Institutes of Health, R01NS091027, K01NS116168. OHSU Fellowship for Diversity in Research, Collins Medical Trust.

Keywords: autism Spectrum disorder | DRG | neuronal differentiation | PTEN | somatosensory

#### **ABSTRACT**

Autism spectrum disorder (ASD) is a complex neurodevelopmental disorder characterized by deficits in social interactions, repetitive behaviors, and hyper- or hyposensitivity to sensory stimuli. The cellular mechanisms underlying the emergence of abnormal sensory sensitivity in ASD are not fully understood. Recent studies in rodent models of ASD identified differences in dorsal root ganglia (DRG) neurons that convey somatosensory information to the central nervous system. However, it is unknown how ASD-associated alterations in DRG neurons emerge during development and if these phenotypes are conserved across ASD models. We examined *Pten* (phosphatase and tensin homolog) heterozygous mice (*Pten*<sup>Het</sup>) as a model for syndromic ASD and identified altered responses to sensory stimuli. Transcriptomic and in vivo analysis identified alterations in subtype-specific markers of DRG neurons in *Pten*<sup>Het</sup> mice, emerging during early DRG development and involving dysregulation of signaling pathways downstream of PTEN. Finally, we show that mice harboring an ASD-associated mutation (*Pten*<sup>Y69H</sup>) show nearly identical alterations in the expression of somatosensory neuron subtype-specific markers. These results show that precise levels of PTEN are required for proper somatosensory development and provide insight into the molecular and cellular basis of sensory abnormalities in a model for syndromic ASD.

#### 1 | Introduction

Altered sensory responsiveness is a defining feature of autism spectrum disorder (ASD) and has been recapitulated in animal models of ASD (Tomchek and Dunn 2007; Cascio 2010; Monday et al. 2023). While much of the research has focused on sensory processing regions of the brain, recent advances show that altered function of primary sensory neurons is frequently seen in models for ASD. Multiple groups have reported alterations in retinal (Vlasits et al. 2025), auditory (McChesney et al. 2022), and somatosensory circuits (Huzard et al. 2024; Orefice et al. 2016, 2019; Tasnim et al. 2024; Bhattacherjee, Mu, et al. 2017). Despite

the progress made on characterizing sensory features in animal models of ASD, how these defects emerge during development remains understudied.

Somatosensory information is conveyed from the periphery to the CNS by primary neurons in the dorsal root ganglia (DRG). In the developing mouse embryo, DRG neurons are derived from neural crest cells that coalesce into ganglia, proliferate, and differentiate into distinct subtypes of neurons between embryonic days 9.5 and 14.5 (E9.5-E14.5) (Landy et al. 2021; Ma et al. 1999). One of the earliest distinctions between DRG neuron subtypes is their expression of different Trk receptors. Neurons expressing

This is an open access article under the terms of the Creative Commons Attribution-NonCommercial License, which permits use, distribution and reproduction in any medium, provided the original work is properly cited and is not used for commercial purposes.

© 2025 The Author(s). Autism Research published by International Society for Autism Research and Wiley Periodicals LLC.

#### Summary

- Abnormal sensory sensitivity is a feature of autism spectrum disorder (ASD).
- We examined mice lacking a single copy of Pten as a model of ASD and identified altered sensory behaviors accompanied by defects in the development of peripheral sensory neurons.
- These results provide new insights into the developmental mechanisms underlying sensory phenotypes in ASD.

TrkC and/or TrkB are typically medium and large diameter neurons, whereas TrkA is expressed in small diameter neurons (Marmigere and Ernfors 2007). Neurotrophin signaling through Trk receptors controls the survival, differentiation, and maturation of DRG neurons. As DRG neurons extend an axon to targets in the periphery and into the developing spinal cord, neurotrophins derived from intermediate and final targets support their survival (Crowley et al. 1994; Patel et al. 2000). Approximately 50% of DRG neurons undergo apoptotic cell death during this window, ensuring that the appropriate number of neurons innervate the correct targets (Snider 1994).

DRG subtype diversification begins embryonically and continues through the first 2 weeks of life. There are ~15 genetically distinct subtypes of somatosensory neurons that respond to a wide range of physiological stimuli (Sharma et al. 2020; Meltzer et al. 2021; Usoskin et al. 2015; Li et al. 2016). Proprioceptive neurons are comprised of three subtypes of large diameter neurons that innervate muscle spindles and Golgi tendon organs (Arber et al. 2000). Large diameter Aβ-low threshold mechanoreceptors (LTMRs) innervating targets in the skin can be subdivided into multiple rapidly adapting (RA) and slowly adapting (SA) subtypes (Li et al. 2011; Abraira and Ginty 2013). Aβ-LTMR subtypes are differentially responsive to hair deflection, vibration, and pressure, and can be distinguished by their morphologically distinct endings in the skin around hair follicles or in association with specialized Merkel cells or Pacinian corpuscles (Belkaid and Segre 2014; Bai et al. 2015). Medium diameter populations of DRG neurons include Aδ-LTMR neurons that respond to hair deflection (Rutlin et al. 2014) and high threshold mechanoreceptors (HTMRs) (Ghitani et al. 2017; Arcourt et al. 2017). Small diameter neuron subtypes in the DRG include C-LTMRs that detect light touch in hairy skin and nociceptors that detect painful or noxious stimuli (Li et al. 2011; Seal et al. 2009; Cavanaugh et al. 2009; Zylka et al. 2005). The multiple subtypes of nociceptive neurons have classically been divided into TrkA+ peptidergic subtypes that express CGRP and Substance P and Ret+ non-peptidergic neurons (Basbaum et al. 2009).

Recent work has identified abnormal primary somatosensory neuron function in multiple models of syndromic ASD (Huzard et al. 2024; Orefice et al. 2016, 2019; Tasnim et al. 2024; Bhattacherjee, Mu, et al. 2017). Mice with heterozygous deletion or mutation of *Mecp2*, *Fmr1*, *Shank3b*, or *Gabrb3* all exhibit altered responses to tactile stimuli (Huzard et al. 2024; Orefice et al. 2016, 2019; Tasnim et al. 2024; Bhattacherjee, Mu, et al. 2017; Bhattacherjee, Winter, et al. 2017; Zimmerman

et al. 2019; DeLorey et al. 2011). These effects are DRGautonomous and involve alterations in presynaptic gating of sensory information conveyed into the dorsal spinal cord. Mice with heterozygous loss of the ASD-associated genes Nlgn2 or RORβ also show abnormal sensory reactivity, but these genes appear to function in dorsal spinal cord interneurons that control feedforward inhibition onto DRG neurons (Tasnim et al. 2024). One critical distinction of these ASD models is the timing of when phenotypes are observed; Mecp2<sup>-/y</sup> and Gabrb3<sup>+/-</sup> mice show hypersensitivity to an air puff at P4, whereas hypersensitivity to mechanical stimuli in Nlgn2 or ROR\$\beta\$ mutants was not apparent until adulthood (Tasnim et al. 2024). Therefore, there is considerable heterogeneity in both how and when primary sensory neuron abnormalities manifest in distinct models of ASD. Overall, the developmental timing of primary somatosensory neuron alterations in models of ASD is poorly characterized.

Heterozygous mutations in *Phosphatase* and tensin homolog (PTEN) have been identified in ~2% of all ASD cases and represent up to 20% of individuals with ASD and macrocephaly (Frazier 2019). Most PTEN ASD-associated mutations lead to a loss of function of the protein (Mighell et al. 2018). Pathogenic germline mutations in PTEN can lead to several disorders that are encompassed under the umbrella diagnosis of PTEN hamartoma tumor syndrome (PHTS) (Yehia and Eng 2018). In addition to vascular and dermatologic symptoms and increased susceptibility to cancer, PHTS patients show a prevalence of ASD of 22% (Yehia et al. 2020; Busch et al. 2019). Cognitive deficits in PHTS individuals with ASD seem to be more severe than in individuals without ASD (Busch et al. 2019). Sensory phenotypes are common features among PTEN-associated ASD (Marco et al. 2011) and include tactile, taste, and smell sensitivity, as well as hypotonia, constipation, and gastrointestinal disorders (Busch et al. 2019; Busa et al. 2013; Liu et al. 2024). However, the etiology of these sensory phenotypes remains unclear.

Pten haploinsufficiency is a well-established mouse model for syndromic ASD and recapitulates many of the clinical findings of human patients. Mice harboring Pten heterozygous mutations (Pten<sup>+/-</sup>, referred as Pten<sup>Het</sup>) show ASD-related behavioral deficits, including decreased sociability, repetitive behaviors, anxiety, and sensorimotor defects (Clipperton-Allen and Page 2020; Clipperton-Allen et al. 2022). PTEN functions as a dual lipid and protein phosphatase and has many roles in regulating intracellular signaling pathways (Worby and Dixon 2014). One of the best studied functions of PTEN is as the primary negative regulator of the PI3K/AKT/mTOR pathway (Huang and Reichardt 2003; Reichardt 2006; Postigo et al. 2002; York et al. 2000; Philpott et al. 1997; Song et al. 2010). Mutations in several other genes in this pathway, including PIK3CA, MTOR, PPP2R5D, and TSC, are also associated with ASD, implicating PI3K/AKT/mTOR as a critical signaling hub (Yeung et al. 2017; Crino et al. 2006; Gutierrez et al. 1998). In DRG neurons, the PI3K/AKT/mTOR pathway functions downstream of neurotrophin-mediated Trk receptor activation to regulate the survival and differentiation of DRG neurons (Snider and Silos-Santiago 1996; Klesse and Parada 1998; Datta et al. 1997; Aksamitiene et al. 2012; Huang and Reichardt 2001).

Based on its association with ASD and its critical role in regulating an essential pathway in DRG neuron development, we

examined the effects of heterozygous deletion of Pten (Pten<sup>Het</sup>) on primary somatosensory neurons. We find that the loss of a single copy of Pten results in alterations in multiple somatosensory behaviors. Bulk RNAseq analysis of adult DRGs from Pten<sup>Het</sup> mice indicated shifts in the proportion of neuronal subtypes, which were confirmed by analyzing DRG population markers in vivo. We find that these defects manifest at the earliest stages of DRG development and are accompanied by overactivation of both mTOR and GSK3-β signaling cascades downstream of PTEN. In addition, mice harboring a heterozygous ASD-associated mutation that shows predominant nuclear localization (PtenY68H/+) phenocopy defects in DRG marker expression (Lobo et al. 2009; He et al. 2011; Sarn et al. 2021), highlighting the clinical relevance of our model. Taken together, these results show the contribution of PTEN signaling to molecular identity in DRGs, providing insight into the consequences of PTEN mutations and their contribution to sensory features seen in individuals with PTENrelated ASD.

#### 2 | Materials and Methods

#### 2.1 | Mouse Lines

All experiments were approved by the Oregon Health & Science University Institutional Animal Care and Use Committee (Protocol #IS00000539). Animals were housed in standard conditions and cared for by the Department of Comparative Medicine at Oregon Health & Science University. Mice were maintained in a 12-h light/dark cycle and provided food and water ad libitum. For experiments involving embryonic timepoints, noon on the date that a vaginal plug was detected was considered E0.5. For experiments involving constitutive Pten heterozygous mice, male PtenHet breeders (B6;129P2-Pten<sup>tm1Mak</sup>/Mmjax, MMRRC stock #42059 (Suzuki et al. 1998)) were crossed with CD1 females to generate experimental mice on a mixed genetic background. For examining phenotypes related to the patient-specific Y68H Pten mutation, PtenY68H/+ male breeders (Sarn et al. 2021) were crossed to CD1 females to generate experimental mice. We examined activation of the GSK-3β/β-Catenin pathway, using Pten<sup>Het</sup> breeders crossed to a TCF/Lef:H2B-EGFP reporter line (Tg(TCF/Lef1-HIST1H2BB/EGFP)61Hadj/J, MMRRC stock #013752 (Ferrer-Vaquer et al. 2010)). All animals were group housed with littermates and maintained on a mixed genetic background. Mice of both sexes were used for all experiments, and WT littermates were used as controls. All staining in adult animals was performed in 3-week-old littermate mice. Behavioral paradigms were performed in animals between 6 and 10 weeks of age.

#### 2.2 | Behavioral Assays

#### 2.2.1 | Rotarod Test

A standard accelerating rotarod (Harvard Apparatus) with capacity for testing 5 mice simultaneously was used to test 14 wild type and 14 *Pten*<sup>Het</sup> mice (7 males and 7 females of each genotype). Rotator initial rotation velocity was 2.5 RPM and

accelerated by 0.5 RPM/s. The falling mouse landed on a platform connected to a timer, and the time spent on the rotarod was recorded. All mice went through test sessions for 5 consecutive days. Repeated measures ANOVA and Bonferroni post hoc analysis were used to determine statistical differences across genotypes throughout 5 days of testing.

#### 2.2.2 | Adhesive Removal Test

Light touch was assessed as previously described (Bouet et al. 2009). Mice were placed in a plexiglass container, and after a period of acclimation of at least 5 min, a small piece of tape (7 mm diameter) was carefully placed onto the back of the coat of an unrestrained mouse. The animal was observed for 15 min, and the number of responses to the tape stimulus was recorded. Latency to adhesive removal was plotted using Kaplan–Meier curves to evaluate performance differences by genotype, and statistical significance between curves was assessed by logrank test.

#### 2.2.3 | Oil Drop Test

Test was performed as previously described (Zhang et al. 2024). In brief, animals were placed in a plexiglass box where they were allowed to acclimate and explore for 15 min. After the acclimation period, we delivered a  $50\,\mu\text{L}$  drop of sunflower oil (stabilized at room temperature) and behaviors were recorded for 5 min at 240 frames per second (fps). Videos were analyzed at 30 fps, and the number of shakes within the timeframe was counted. Statistical analysis of effects between genotypes was performed using the Wilcoxon test.

#### 2.2.4 | Von Frey Assay

We used a Dynamic Plantar Aesthesiometer (UgoBasile), which has calibrated von Frey fibers and a movable force-actuator, to measure mechanical somatosensation. Animals were enclosed but unrestrained in an acrylic chamber placed over a meshed floor during the duration of the experiments. The actuator was placed below the paw of the animal to confer different degrees of force via a von Frey filament, starting below the threshold of detection and increasing until the paw withdrawal reflex was elicited. Statistical analysis of effects between genotypes was performed using the Wilcoxon test.

#### 2.2.5 | Heat Nociception

Animals were placed in an acrylic box over a grated platform unrestrained during the duration of the experiment. After a 5-minute acclimation period, a blunt probe with a force of 1g was applied to the plantar surface of the animal's hindlimb. The metal probe touched the paw, heating up at a rate of 2.5°C/s to a maximum temperature of 60°C. Animals were monitored, and their reaction times and temperature at the time of withdrawal were recorded. Testing was performed 3 times per animal, with a 60s recovery time between intervals. Statistical analysis of effects between genotypes was performed using the Wilcoxon test.

#### 2.2.6 | Tissue Preparation and RNA Isolation

For transcriptome profiling by RNA sequencing, whole DRGs along the entire rostro-caudal axis from 4 six-week-old animals of each genotype were dissected, collected in 1.5 mL Eppendorf tubes, pelleted, and snap-frozen in dry ice. Frozen tissue was shipped on dry ice to Genewiz (Azenta Life Sciences) for RNA sequencing. The RNA sequencing workflow included RNA isolation, PolyA selection-based mRNA enrichment, mRNA fragmentation, and complementary DNA (cDNA) synthesis. Sequencing of cDNA libraries was performed on the Illumina NovaSeq platform with 2×150-base pair (bp) read length. Reads were aligned to the *Mus musculus* GRCm38 reference genome available on ENSEMBL with STAR aligner v.2.5.2b.

#### 2.2.7 | RNA-Seq Data Analysis

DESeq2 was used for comparison of gene expression levels between different sample groups. p values and  $\log_2$  fold changes were calculated using a Wald test. Genes with adjusted p values  $(P_{adi})$  of < 0.05 were referred as DEGs.

DeconV was used to deconvolute RNA-seq data and infer proportions of DRG subtypes in WT and Pten<sup>Het</sup> (Gynter et al. 2023). DeconV consists of a reference model and a deconvolution model. The reference model learns parameters from single-cell reference, which the deconvolution model uses to infer optimal cell type composition of a bulk sample. We used the adult dataset from Sharma et al. (Sharma et al. 2020) as a single-cell reference, and we compiled bulk samples from Accession number GEO: GSE131230 and GSE162263 (Zheng et al. 2019; Oliver et al. 2021) as the bulk counterpart of the reference sample. DeconV was executed with scripts based on examples provided by the developers. Briefly, we fitted the bulk reference model using the parameters of the singlecell reference to obtain a probabilistic model consisting of a discrete distribution (zero inflated negative-binomial) with cell-type specific parameters for single-cell gene counts. Once the reference model was fitted, the deconvolution model was used to translate expression to real bulk gene expression. Based on the combination of parameters from the reference and deconvolution models, we generated a reference file that was then used as a template to infer subtype proportions in our bulk RNA-seq dataset. Default parameters were used for fitting, modeling, and training of the algorithm.

#### 2.2.8 | Tissue Processing and Immunolabeling

All immunolabeling was performed on cryosections following standard protocols (Pomaville and Wright 2023). Whole mouse embryos, from litters ranging from E9.5 to E14.5, were fixed overnight at 4°C in 4% paraformaldehyde with gentle agitation. For analysis of P21 DRGs, intact spinal columns were first dissected and fixed overnight at 4°C in 4% paraformaldehyde. The next day, spinal columns were washed in PBS for 30 min at room temperature, and spinal cords and attached DRGs were dissected from the spinal column for further processing. All tissue was cryoprotected by incubating in 15% sucrose in PBS for 1 h, followed by 20% sucrose in PBS overnight at 4°C with gentle agitation. Samples were mounted in OCT and rapidly frozen in methylbutane on dry ice. 20  $\mu$ m consecutive sections were cut on

a Leica CM3050S cryostat, mounted on slides, and allowed to dry for 2 h at room temperature.

For immunolabeling, cryosections mounted on slides were washed 3 times for 5 min in PBS at room temperature and incubated for 1 h in blocking solution (5% v/v Normal Donkey Serum, 5% v/v DMSO, 0.25% v/v Triton X-100 in PBS). Slides were then incubated in primary antibodies diluted in blocking solution overnight at 4°C in a humidified staining box. Concentrations for primary antibodies are listed on Table 1. Slides were then washed three times for 5 min in PBS and incubated for 2h at room temperature in secondary antibodies diluted at 1:500 in blocking solution. EdU incorporation was detected using Click-iT EdU Cell Proliferation Kit for Imaging, Alexa Fluor 647 (Thermo Fisher Scientific, Cat#C10340). Slides were incubated in EdU detection solution (100 µM Tris pH7.5, 4mM CuSO<sub>4</sub>, 5µM sulfo-Cy5 azide, 100mM sodium ascorbate) for 30 min at RT, protected from light. Slides were washed 3 times for 10min in PBS, with 1:5000 Hoechst added to the second wash to label nuclei. Slides were then coverslipped with Fluoromount-G and imaged.

#### 2.2.9 | Proliferation Assays

A single intraperitoneal (IP) injection of EdU in sterile PBS ( $10 \mu g$  EdU/g body weight) was given to pregnant dams on 1 day between E9.5 and E14.5. Two hours after injection, embryos were collected and fixed as described.

#### 2.2.10 | Cell Counts and Statistical Analysis

To quantify immunoreactive DRG neurons, level-matched DRGs from lumbar segments were serially sectioned. For the analysis of the total number of neurons, sections of entire DRGs were counted. \\ For population proportions, cell proliferation, and cell death assays, 5 consecutive sections of level-matched DRGs were counted. Sections were immunostained with antibodies against specific cell markers and Isl1/2. The proportions of each population were calculated by dividing the number of marker-positive cells by the number of total neurons in serial sections from level-matched DRGs of control and mutant mice. Values were averaged for each experiment, with a minimum of 5 animals of mixed sex for each genotype at each timepoint and condition across different litters. The average ± SEM is reported in the figures. Statistical analysis of adults was performed using the Wilcoxon rank-sum test, with Bonferroni correction applied for post hoc comparisons. Analysis of phenotypes during developmental time points was performed using 2-way ANOVA followed by Tukey's HSD post hoc pair-wise comparisons with correction for multiple testing.

#### 3 | Results

### 3.1 | Alterations in *Pten* Lead to Somatosensory Defects

Germline heterozygous mutations in *PTEN* are associated with ASD, and mouse models carrying these mutations display a range of behavioral phenotypes (Busch et al. 2019; Clipperton-Allen and Page 2020; Uljarevic et al. 2021; Hansen-Kiss

TABLE 1 | Antibodies used.

Antibody	Species	Supplier	Cat #	RRID	Concentration
		Primary antibodies			
Calbindin	Rabbit	Swant	CB 38	AB_10000340	1:1000
Tyrosine hydroxylase (TH)	Rabbit	Millipore	AB152	AB_390204	1:1000
TrkA	Goat	Fisher (R&D systems)	AF1056	AB_2283049	1:100
TrkB	Goat	Fisher (R&D systems)	AF1494	AB_2155264	1:100
TrkC	Goat	Fisher (R&D systems)	AF1404	AB_2155412	1:100
Casp3	Rabbit	Cell signaling	9661S	AB_2341188	1:500
CGRP	Igg2a	Abcam	ab81887	AB_1658411	1:300
Etv1	Rabbit	Invitrogen	PA5-77975	AB_2735767	1:250
Anti-Kv4.3 K+ channel antibody (K75/41)	Igg1	Antibodies Inc	75-017	AB_2131966	1:500
Isl1/2	Mouse Igg2b	DHSB	39.4D5	AB_2314683	1:250
GFP	Chicken	Abcam	ab13970	AB_300798	1:1000
		Secondary antibodies			
Anti-Rabbit IgG 488	Donkey	Thermo fisher scientific	A-21206		1:500
Anti-Rabbit IgG 546	Donkey	ThermoFisher	A10040		1:500
Anti-Rabbit IgG 647	Donkey	ThermoFisher	A-31573		1:500
Anti-Mouse Igg2b 488	Goat	ThermoFisher	A-21141		1:500
Anti-Chicken IgY 488	Donkey	Jackson immuno research	NC0215979		1:500
Anti-Goat 647	Donkey	ThermoFisher	A-21447		1:500

et al. 2017). However, the somatosensory consequences of *Pten* haploinsufficiency remain insufficiently characterized. We therefore conducted a battery of sensory assays targeting proprioception, mechanosensation, and nociception to evaluate sensory function in WT and *Pten*<sup>Het</sup> mice (Figure 1A).

We first assessed sensorimotor coordination using the accelerating rotarod assay. In males,  $Pten^{Het}$  mice displayed significantly reduced latency to fall on days four and five relative to WT littermates, indicating impaired motor performance (Figure 1B).  $Pten^{Het}$  females showed no statistically significant difference compared to WT controls with the exception of day 1, during which they showed a reduced latency to fall (Figure 1C). These results suggest a sex-dependent impact of Pten haploinsufficiency on motor learning and coordination, with males more severely affected.

To evaluate tactile-motor integration, we employed the adhesive removal test and analyzed latency to sticker removal using Kaplan–Meier curves (Nolan et al. 2019). Male  $Pten^{Het}$  mice exhibited a significant response delay compared to WT controls ( $p\!=\!0.019$ ; Figure 1D), suggesting deficits in somatosensory processing and/or response initiation. A similar delay was observed in females ( $p\!=\!0.029$ ; Figure 1E). These findings indicate that Pten haploinsufficiency impairs sensorimotor responses in both sexes.

Next, we probed C-LTMR-mediated mechanosensation using an oil droplet stimulus applied to the hairy skin of the neck, which evokes "wet dog shakes" (WDS) via a spinoparabrachial pathway (Zhang et al. 2024). Both male and female  $Pten^{Het}$  mice exhibited a significantly greater number of WDS bouts compared to sex-matched WT littermates (p=0.007 and p=0.01, respectively; Figure 1F), indicating that Pten loss enhances C-LTMR-evoked sensorimotor responses in both sexes.

To assess mechanical sensitivity, we conducted the Von Frey assay. Pten<sup>Het</sup> male mice and female mice showed significantly lower withdrawal thresholds compared to sex-matched WT littermates (p=0.011 and p=0.0097, respectively; Figure 1G). Responses in PtenHet mice were elicited by low-force filaments ranging 0.4-1.4g, whereas WT mice responded to filaments in the 2-8 g range, indicating pronounced mechanical hypersensitivity in both sexes. Thermal nociception was evaluated using the thermal probe assay, applying a ramped heat stimulus to the plantar hind paw. PtenHet male and female mice exhibited significantly lower withdrawal temperatures compared to sexmatched WT littermates (p = 0.0012 and p = 0.0087, respectively; Figure 1H). Together, these results reveal that Pten<sup>Het</sup> mice exhibit complex alterations in somatosensory behavior. Across multiple modalities, Pten haploinsufficiency results in hypersensitivity to certain stimuli (e.g., mechanical and thermal),

19393806, 2025, 11, Downloaded from https://onlinelibrary.wiley.com/doi/10.1002/aur.70119 by CASE WESTERN RESERVE UNIVERSITY, Wiley Online Library on [28/11/2025]. See the Terms

on Wiley Online Library for rules of use; OA articles are governed by the applicable Creative Commons License

Autism Research, 2025 2197

FIGURE 1 | Behavioral abnormalities in different sensory modalities in PtenHet mutants, (A) Timeline of behavioral paradigms and schematic of each test performed. (B and C) Quantification of sensorimotor performance in accelerating rotarod experiment in males (B) (n=7) animals per genotype across 4 litters; Day 1: 20.4 ± 3.2 s in WT vs. 17.4 ± 3.1 s in Pten<sup>Het</sup>, repeated measures ANOVA, Bonferroni correction p.adj = 0.51600; day  $2: 29.5 \pm 3.8 \text{ s in WT vs. } 21.1 \pm 2.5 \text{ s in } Pten^{Het}, \text{ p.adj} = 0.09780; \text{ day } 3: 43.9 \pm 5.4 \text{ s in WT vs. } 27.9 \pm 5.1 \text{ s in } Pten^{Het}, \text{ p.adj} = 0.05310; \text{ day } 4: 40.9 \pm 5.3 \text{ s in WT vs. } 27.9 \pm 5.1 \text{ s in } Pten^{Het}, \text{ p.adj} = 0.05310; \text{ day } 4: 40.9 \pm 5.3 \text{ s in WT vs. } 27.9 \pm 5.1 \text{ s in } Pten^{Het}, \text{ p.adj} = 0.05310; \text{ day } 4: 40.9 \pm 5.3 \text{ s in WT vs. } 27.9 \pm 5.1 \text{ s in } Pten^{Het}, \text{ p.adj} = 0.05310; \text{ day } 4: 40.9 \pm 5.3 \text{ s in WT vs. } 27.9 \pm 5.1 \text{ s in } Pten^{Het}, \text{ p.adj} = 0.05310; \text{ day } 4: 40.9 \pm 5.3 \text{ s in WT vs. } 27.9 \pm 5.1 \text{ s in } Pten^{Het}, \text{ p.adj} = 0.05310; \text{ day } 4: 40.9 \pm 5.3 \text{ s in WT vs. } 27.9 \pm 5.1 \text{ s in } Pten^{Het}, \text{ p.adj} = 0.05310; \text{ day } 4: 40.9 \pm 5.3 \text{ s in } Pten^{Het}, \text{ p.adj} = 0.05310; \text{ day } 4: 40.9 \pm 5.3 \text{ s in } Pten^{Het}, \text{ p.adj} = 0.05310; \text{ day } 4: 40.9 \pm 5.3 \text{ s in } Pten^{Het}, \text{ p.adj} = 0.05310; \text{ day } 4: 40.9 \pm 5.3 \text{ s in } Pten^{Het}, \text{ p.adj} = 0.05310; \text{ day } 4: 40.9 \pm 5.3 \text{ s in } Pten^{Het}, \text{ p.adj} = 0.05310; \text{ day } 4: 40.9 \pm 5.3 \text{ s in } Pten^{Het}, \text{ p.adj} = 0.05310; \text{ day } 4: 40.9 \pm 5.3 \text{ s in } Pten^{Het}, \text{ p.adj} = 0.05310; \text{ day } 4: 40.9 \pm 5.3 \text{ s in } Pten^{Het}, \text{ p.adj} = 0.05310; \text{ day } 4: 40.9 \pm 5.3 \text{ s in } Pten^{Het}, \text{ p.adj} = 0.05310; \text{ day } 4: 40.9 \pm 5.3 \text{ s in } Pten^{Het}, \text{ p.adj} = 0.05310; \text{ day } 4: 40.9 \pm 5.3 \text{ s in } Pten^{Het}, \text{ p.adj} = 0.05310; \text{ day } 4: 40.9 \pm 5.3 \text{ s in } Pten^{Het}, \text{ p.adj} = 0.05310; \text{ day } 4: 40.9 \pm 5.3 \text{ s in } Pten^{Het}, \text{ p.adj} = 0.05310; \text{ day } 4: 40.9 \pm 5.3 \text{ s in } Pten^{Het}, \text{ p.adj} = 0.05310; \text{ day } 4: 40.9 \pm 5.3 \text{ s in } Pten^{Het}, \text{ p.adj} = 0.05310; \text{ day } 4: 40.9 \pm 5.3 \text{ s in } Pten^{Het}, \text{ p.adj} = 0.05310; \text{ day } 4: 40.9 \pm 5.3 \text{ s in } Pten^{Het}, \text{ p.adj} = 0.05310; \text{ day } 4: 40.9 \pm 5.3 \text{ s in } Pten^{Het}, \text{ p.adj} = 0.05310; \text{ day } 4: 40.9 \pm 5.3 \text{ s in } Pten^{Het}, \text{ p.adj} = 0.05310; \text{ day } 4: 40.9 \pm 5.3 \text{ s in } Pten^{Het}, \text{$ WT vs.  $22.6 \pm 2.5$  in  $Pten^{Het}$ , p.adj = 0.00938; day 5:  $37.8 \pm 1.9$  s in WT vs.  $22.2 \pm 3.1$  s in  $Pten^{Het}$ , p.adj = 0.00116;  $Pten^{Het}$ ) and females (C) (n = 7 animals 1 + 1.9 s)per genotype across 4 litters; Day 1:  $31.9 \pm 3.4$ s in WT vs.  $21.2 \pm 3.2$ s in  $Pten^{Het}$ , p. adj = 0.0460; day 2:  $32.8 \pm 4.2$ s in WT vs.  $22.3 \pm 2.6$ s in  $Pten^{Het}$ , p.  $adj = 0.0730; day \ 3: \ 38.6 \pm 5.4 s \ in \ WT \ vs. \ 29.9 \pm 5.1 s \ in \ Pten^{Het}, \ p.adj = 0.2240; day \ 4: \ 41.0 \pm 5.3 s \ in \ WT \ vs. \ 29.2 \pm 2.5 \ in \ Pten^{Het}, \ p.adj = 0.2230; day \ 5: \ 4.0 \pm 5.3 s \ in \ WT \ vs. \ 29.2 \pm 2.5 \ in \ Pten^{Het}, \ p.adj = 0.2230; day \ 5: \ 4.0 \pm 5.3 s \ in \ WT \ vs. \ 29.2 \pm 2.5 \ in \ Pten^{Het}, \ p.adj = 0.2230; day \ 5: \ 4.0 \pm 5.3 s \ in \ WT \ vs. \ 29.2 \pm 2.5 \ in \ Pten^{Het}, \ p.adj = 0.2230; day \ 5: \ 4.0 \pm 5.3 s \ in \ WT \ vs. \ 29.2 \pm 2.5 \ in \ Pten^{Het}, \ p.adj = 0.2230; day \ 5: \ 4.0 \pm 5.3 s \ in \ WT \ vs. \ 29.2 \pm 2.5 \ in \ Pten^{Het}, \ p.adj = 0.2230; day \ 5: \ 4.0 \pm 5.3 s \ in \ WT \ vs. \ 29.2 \pm 2.5 \ in \ Pten^{Het}, \ p.adj = 0.2230; day \ 5: \ 4.0 \pm 5.3 s \ in \ WT \ vs. \ 29.2 \pm 2.5 \ in \ Pten^{Het}, \ p.adj = 0.2230; day \ 5: \ 4.0 \pm 5.3 s \ in \ WT \ vs. \ 29.2 \pm 2.5 \ in \ Pten^{Het}, \ p.adj = 0.230; day \ 5: \ 4.0 \pm 5.3 s \ in \ WT \ vs. \ 29.2 \pm 2.5 \ in \ Pten^{Het}, \ p.adj = 0.230; day \ 5: \ 4.0 \pm 5.3 s \ in \ WT \ vs. \ 29.2 \pm 2.5 \ in \ Pten^{Het}, \ p.adj = 0.230; day \ 5: \ 4.0 \pm 5.3 s \ in \ WT \ vs. \ 29.2 \pm 2.5 \ in \ Pten^{Het}, \ p.adj = 0.230; day \ 5: \ 4.0 \pm 5.3 s \ in \ WT \ vs. \ 29.2 \pm 2.5 \ in \ Pten^{Het}, \ p.adj = 0.230; day \ 5: \ 4.0 \pm 5.3 s \ in \ WT \ vs. \ 29.2 \pm 2.5 \ in \ Pten^{Het}, \ p.adj = 0.230; day \ 5: \ 4.0 \pm 5.3 s \ in \ Pten^{Het}, \ p.adj = 0.230; day \ 5: \ 4.0 \pm 5.3 s \ in \ Pten^{Het}, \ p.adj = 0.230; day \ 5: \ 4.0 \pm 5.3 s \ in \ Pten^{Het}, \ p.adj = 0.230; day \ 5: \ 4.0 \pm 5.3 s \ in \ Pten^{Het}, \ p.adj = 0.230; day \ 5: \ 4.0 \pm 5.3 s \ in \ Pten^{Het}, \ p.adj = 0.230; day \ 5: \ 4.0 \pm 5.3 s \ in \ Pten^{Het}, \ p.adj = 0.230; day \ 5: \ 4.0 \pm 5.3 s \ in \ Pten^{Het}, \ p.adj = 0.230; day \ 5: \ 4.0 \pm 5.3 s \ in \ Pten^{Het}, \ p.adj = 0.230; day \ 5: \ 4.0 \pm 5.3 s \ in \ Pten^{Het}, \ p.adj = 0.230; day \ 5: \ 4.0 \pm 5.3 s \ in \ Pten^{Het}, \ p.adj = 0.230; day \ 5: \ 4.0 \pm 5.3 s \ in \ Pten^{Het}, \ p.adj = 0.230; day \ 5: \ 4.0 \pm 5.3 s \ in \ Pten^{Het}, \ p.ad$ 38.4±5.2s in WT vs. 24.9±4.7s in Pten<sup>Het</sup>, p.adj = 0.0790; Pten<sup>Het</sup>). (D and E) Quantification of adhesive removal experiment in male (D) and female (E) Pten<sup>Het</sup> mutants. Kaplan–Meier curves show proportion of animals removing sticker over time, where x-axis represent time (in seconds) and yaxis represent the proportion of animals who have not removed the sticker in male mice (D) (n = 7 animals per genotype across 4 litters, log-rank test, p = 0.019) and female mice (E) (n = 7 animals per genotype across 4 litters, log-rank test, p = 0.029). (F) Quantification of the oil droplet experiment, in which an oil drop is applied to the back of the neck of a mouse to elicit mechanosensory responses from C-LTMRs (male mice: 10.8 ± 0.88 shakes in WT vs.  $17.4 \pm 1.2$  shakes in  $Pten^{Het}$ , n = 7 WT/7  $Pten^{Het}$ , Wilcoxon test, p = 0.007; female mice:  $10.81 \pm 1.0$  shakes in WT vs.  $17.4 \pm 1.4$  shakes in  $Pten^{Het}$ , n = 7 WT/7  $Pten^{Het}$ , p = 0.01). (G) Quantification of Von Frey filament experiment to measure mechanosensory responses to skin indentation in hind paw (male mice:  $4.8 \pm 0.96$  g in WT vs.  $1.5 \pm 0.7$  g in  $Pten^{Het}$ , n = 7 WT/7  $Pten^{Het}$ , Wilcoxon test, p = 0.011; female mice:  $4.8 \pm 0.8$  g in WT vs.  $1.5 \pm 0.4 \,\mathrm{g}$  in  $Pten^{Het}$ ,  $n = 7 \,\mathrm{WT}/7 \,Pten^{Het}$ , p.adj = 0.0097). (H) Quantification of threshold to hind paw withdrawal in response to thermal stimuli (male mice:  $41.7^{\circ}$ C  $\pm 1.6^{\circ}$ C in WT males vs.  $55.0^{\circ}$ C  $\pm 0.8^{\circ}$ C in  $Pten^{Het}$ , n=7 WT/7  $Pten^{Het}$ , Wilcoxon test p=0.0012. Female mice:  $46.4^{\circ}$ C  $\pm 1.9^{\circ}$ C in WT vs.  $54.3^{\circ}\text{C} \pm 0.9^{\circ}\text{C}$  in  $Pten^{Het}$ ,  $n = 7 \text{ WT}/7 Pten^{Het}$ , p = 0.0087).

impaired sensorimotor integration, and sex-dependent deficits in motor coordination.

### 3.2 | Transcriptional Profiles of DRGs Are Altered in $Pten^{Het}$ Mice

A recent study showed that homozygous deletion of *Pten* from adult DRGs results in altered itch behavior due to the upregulation of multiple itch-related genes (Hu et al. 2022). To more comprehensively understand how germline heterozygous deletion of Pten affects gene expression in DRGs, we performed bulk RNA-sequencing (RNA-seq) of whole DRGs isolated from adult PtenHet and WT littermate control mice (Figure 2A). At a Log2 fold change (LFC) threshold of expression at 1.5, we identified 6 differentially expressed genes (DEG) in Pten<sup>Het</sup> mutant mice relative to WT, with 4 genes upregulated and 2 genes downregulated (Figure 2B and Table S1). Overall gene expression changes were relatively small, with many other DEGs either up- or downregulated by < 1.5 LFC (Figure 2C). This relatively small change in gene expression is consistent with studies that have examined the effect of single copy deletion or mutation of Pten in other neuronal populations (Sarn et al. 2021; Cheung et al. 2023). Gene Ontology (GO) analysis of all DEGs identified significant changes to gene networks involved in metabolism, RNA processing, signal transduction, and the ubiquitination pathway (Figure 2D). Surprisingly, Pten was slightly upregulated in mutant DRG samples, potentially due to compensatory autoregulation or altered distribution of Pten expression throughout DRG subtypes (Worby and Dixon 2014).

DRGs exhibit considerable subtype heterogeneity reflecting their multimodal functions (Qi et al. 2024). To determine whether *Pten* heterozygous deletion had a cell-type specific effect in DRG neurons, we integrated our bulk RNA-seq data with an available adult DRG scRNAseq dataset (Sharma et al. 2020). We used estimated DRG subtype proportions in our bulk RNA-seq data along with RNA-seq deconvolution to examine population-specific defects in *Pten*<sup>Het</sup> mutants using DeconV. This deconvolution algorithm leverages gene

expression profiles from a reference sample along with probability distributions to infer the proportional abundance of distinct cell types within a target bulk RNA-seq sample (Gynter et al. 2023) (Figure 2E). This approach detected a potentially altered distribution of DRG subtype transcriptomes in *Pten*<sup>Het</sup> mutants when compared to controls, particularly in populations of C-LTMRs, peptidergic nociceptors, and proprioceptors (Figure 2F).

## 3.3 | DRG Subtype-Specific Marker Expression Is Altered in $Pten^{Het}$ Mice

Based on the DeconV prediction of altered DRG subtype proportions in Pten<sup>Het</sup> mutants, we evaluated DRG subtype populations in vivo. We collected hindlimb-innervating DRGs (lumbar level 3-4; L3-L4) from P21 PtenHet mutants and WT control littermates and quantified the various DRG populations using subtype-specific markers (Figure 3A). Most population subtypes within DRGs are transcriptionally and functionally matured by P21; therefore, allowing correlations of our immunohistochemical data to behavioral and sequencing data from adult animals (Tasnim et al. 2024; Sharma et al. 2020). We found no difference in the total number of Isl1/2+ DRG neurons between mutants and controls (n = 3 animals per genotype, Figure 3B). In contrast, we identified alterations in the proportion of DRG neuron subtypespecific markers in PtenHet mutants, with some populations affected while others were spared (n=5 animals per genotype; 3 males/2 females). There was a significant increase in Tyrosine Hydroxylase positive (TH+) C-LTMRs (156% increase) and TrkC+ proprioceptors (56% increase) in PtenHet mutants. TrkA+ peptidergic nociceptors were reduced by 53% in Pten<sup>Het</sup> mutants relative to WT littermates, whereas IB4+ non-peptidergic nociceptors were unaffected. On the other hand, Calbindin positive (CB+) Aβ-LTMRs and TrkB+ Aδ-LTMRs were unaffected in PtenHet mutants (Figure 3A,C). The alterations in TH+, TrkC+, and TrkA+ populations could arise from misexpression of the specific markers used to identify these neuronal subtypes or changes in subtype diversification during development. To distinguish between these possibilities, we analyzed each of these populations with secondary subtype-specific markers: Cav4.1 for TH+ C-LTMRs,

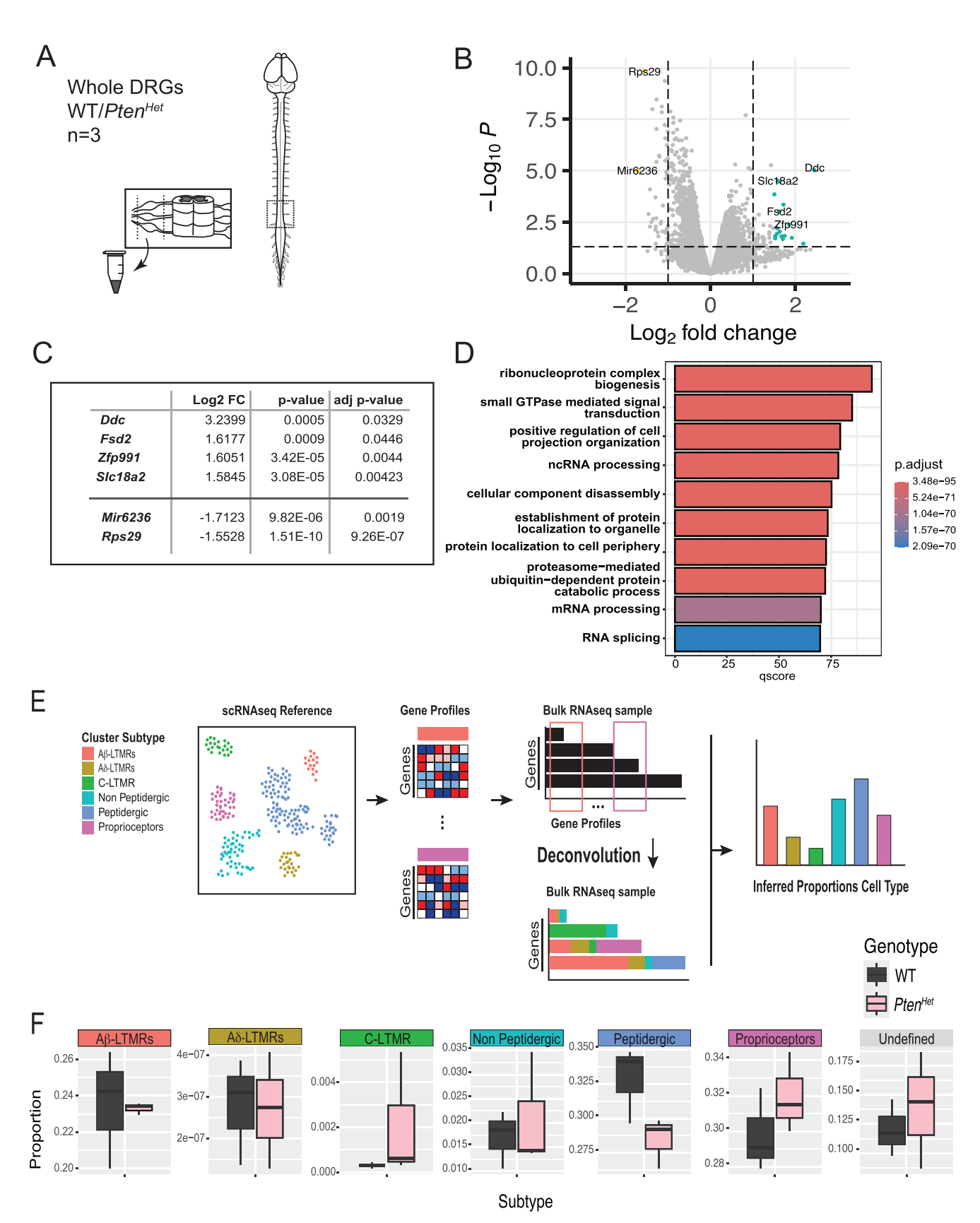


FIGURE 2 | Legend on next page.

Etv1 for TrkC+ proprioceptors, and CGRP for TrkA+ peptidergic nociceptors. We found that primary and secondary subtype markers showed comparable colocalization for each population

in *Pten*<sup>Het</sup> mutants and wildtype littermates (Figure S1). These results suggest that the loss of a single copy of *Pten* likely causes defects in subtype-specific diversification.

**FIGURE 2** | Altered transcriptome in DRGs from  $Pten^{Het}$  mutants. (A) Schematic of experimental design. Whole DRGs along the entire rostrocausal axis were dissected from  $Pten^{Het}$  mutants and WT littermates and processed for bulk RNA sequencing (RNAseq). (B) Volcano plot highlighting genes that are significantly upregulated (4 genes, LFC > 1.5, turquoise, right) and downregulated (2 genes, LFC < -1.5, yellow, left) in  $Pten^{Het}$  mutants (adjusted p value < 0.05). (C) List of top differentially expressed genes (top upregulated genes on top, top downregulated genes bottom, LFC > 1.5 and < -1.5). (D) Barplot showing Gene Ontology analysis for differentially expressed genes. Bars are color-coded from blue to red based on the adjusted p-value. (E) Computational framework to infer proportions of DRG subtypes from RNA-seq data using DeconV (Gynter et al. 2023). scRNA-seq data containing expression profiles from each DRG population subtype is used as a reference dataset (left). Gene profiles for each population are extracted and the probabilistic framework of DeconV is used to estimate proportions of each subtype, based on an assumed linear-sum-property between single-cell and bulk gene expression (middle). DeconV then provides the proportions of each subtype as an output (right). (F) Inferred quantification of DRG population subtypes in WT and  $Pten^{Het}$  by probabilistic cell type deconvolution. Quantification suggests alterations to distribution of C-LTMRs, peptidergic nociceptors, and proprioceptor populations in  $Pten^{Het}$  mutants.

### 3.4 | Early DRG Development Is Abnormal in $Pten^{Het}$ Mutants

We next sought to determine whether sensory neuron subtype differentiation was altered during development in Pten<sup>Het</sup> mutants by using well-established early neuronal markers of nociceptive (TrkA), mechanoreceptive (TrkB), and proprioceptive (TrkC) lineages that are expressed during the critical window of sensory neuron fate determination (Sharma et al. 2020; Huang and Reichardt 2001; Keeler et al. 2022). Analysis of TrkA expressing neurons revealed genotype-dependent differences, with Pten<sup>Het</sup> mice exhibiting significantly reduced proportions compared to WT littermates at all time points (Figure 4B), suggesting that Pten haploinsufficiency strongly impairs TrkA lineage specification throughout development. For TrkB, there were no significant differences in proportions between WT and PtenHet mice at any time point (p > 0.05 for all comparisons, Figure 4C). In contrast, analvsis of TrkC neurons revealed that PtenHet mice had significantly higher proportions compared to WT littermates between E10.5 and E12.5 (Figure 4D). These findings indicate that the loss of a single allele of Pten affects TrkC differentiation during early DRG development, in a direction opposite to that observed for TrkA.

We then examined whether changes in cell proliferation or developmental apoptosis contributed to the alterations in DRG subtype proportions using EdU birth dating and activated Caspase-3 staining, respectively. We observed no significant differences in neuronal progenitor proliferation or developmental apoptosis between *Pten*<sup>Het</sup> mutants and WT littermates in developing DRGs at any of the time points examined (Supplemental Figure 2). These results suggest that appropriate levels of Pten are critical for the proper differentiation of DRG subtypes.

## 3.5 | Downstream Signaling Pathways Are Altered in $Pten^{Het}$ Mutants

Given that *Pten* haploinsufficiency has distinct effects on developing DRG subtypes, we reasoned that signaling cascades downstream of PTEN could potentially be differentially impacted. PTEN is the primary negative regulator of PI3K/AKT signaling and modulates the activity of both the TSC/mTOR/S6 pathway and the GSK-3 $\beta$ / $\beta$ -catenin pathway (Georgescu 2010; Huang et al. 2007; Chen et al. 2015) (Figure 5A). We examined the proportions of DRG neurons engaged in each signaling cascade at E11.5, using phosphoS6 (pS6) immunostaining as a readout of TSC/mTOR pathway activity. We used a *TCF*/

*Lef:H2B-GFP* reporter mouse that provides a readout of WNT/  $\beta$ -catenin signaling activity to examine GSK-3 $\beta$ / $\beta$ -catenin activation (Ferrer-Vaquer et al. 2010). We found an increased proportion of Isl1+ neurons that were positive for both pS6 and GFP in *Pten*<sup>Het</sup> mutants when compared to WT (Figure 5B,C). Closer examination of each DRG subtype revealed population-specific activation of PTEN-dependent downstream signaling. Both TrkA+ and TrkC+ neuronal subtypes showed a significant increase in the proportion of neurons positive for pS6, while there was no change in the proportion of pS6+ TrkB+ neurons (Figure 5D-G). In contrast, only the TrkC+ population had a significantly increased proportion of GFP+ neurons indicative of Gsk-3 $\beta$ / $\beta$ -catenin activation. These results provide evidence for subtype-specific alterations of signaling cascades due to *Pten* haploinsufficiency during DRG development.

### 3.6 | DRG Neuron Diversification Is Abnormal in Mice With an ASD-Associated Mutation in *Pten*

Given the prevalence of PTEN mutations within the ASD population and the high incidence of sensory phenotypes in ASD (Tilot et al. 2015; Ben-Sasson et al. 2009), we examined DRG subtype markers in a mouse model carrying a patient-specific PTEN mutation (PtenY68H/+). This mutation affects the phosphatase domain and results in reduced protein stability and phosphatase activity, and predominantly nuclear localization in CNS neurons (Mighell et al. 2018; Sarn et al. 2021; Han et al. 2000). We found that *Pten*<sup>Y68H/+</sup> mice have alterations in DRG subtype proportions that mirror our results in PtenHet mutants. There was a significant increase in TH+ C-LTMRs (60% increase) and TrkC+ neurons (77% increase) in PtenY68H/+ mice when compared to WT littermates. The proportion of TrkA<sup>+</sup> peptidergic nociceptors was reduced by 44%, whereas the population of IB4+ non-peptidergic nociceptors was unaffected. In contrast, there was no change in the proportion of CB<sup>+</sup> Aβ LTMRs or TrkB<sup>+</sup> Aδ-LTMRs (Figure 6A,B). The nearly identical phenotypes of PtenY68H/+ mice and PtenHet mice highlight the clinical relevance of our findings that identify a critical role for precise PTEN levels in regulating DRG development and the expression of subtype-specific markers.

#### 4 | Discussion

PTEN is the primary negative regulator of PI3K/AKT signaling and has been extensively studied for its role in the development, function, and regeneration of the nervous system. However,

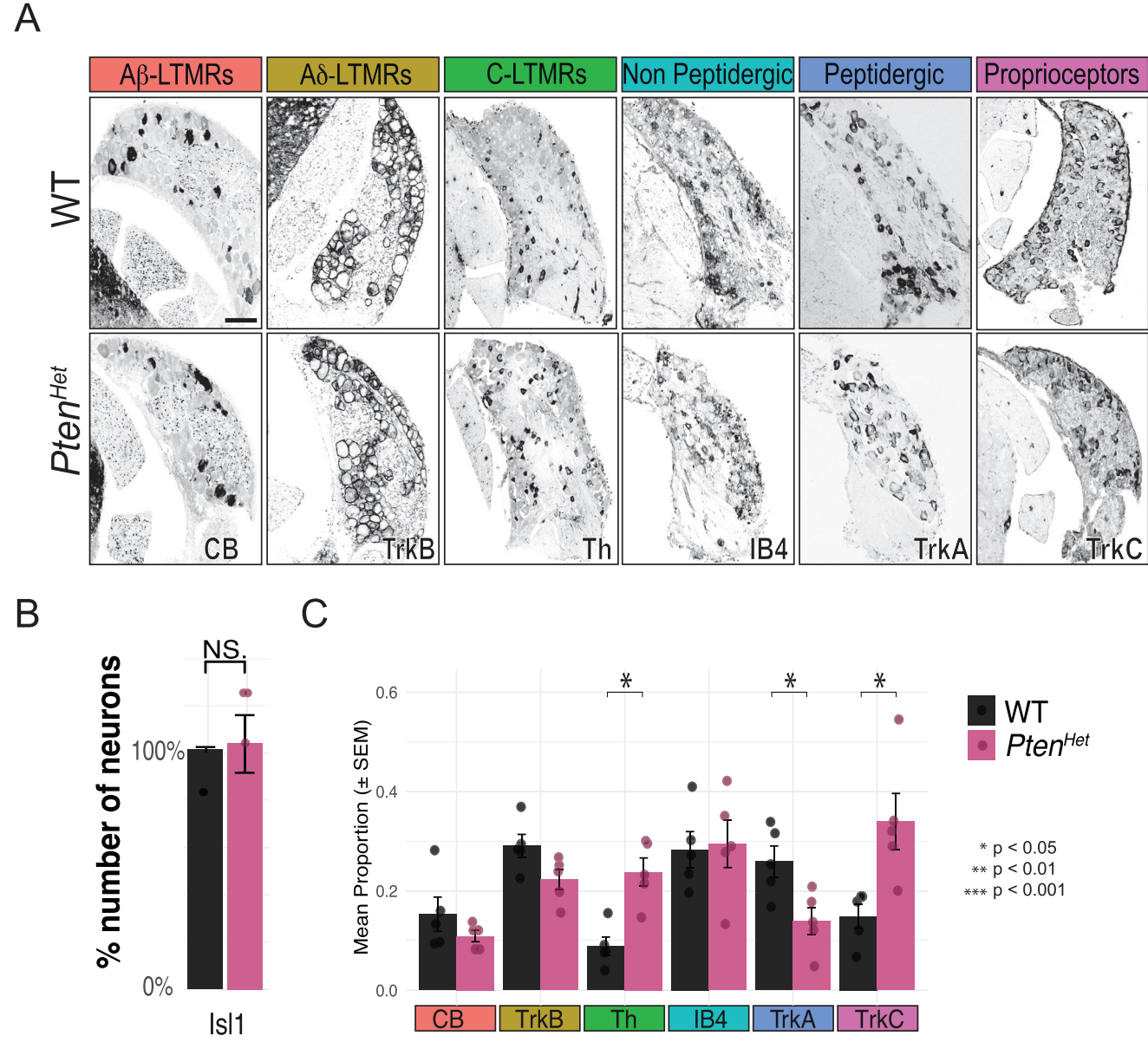


FIGURE 3 | Expression of subtype-specific markers is altered in  $Pten^{Het}$  mutants (A) Representative images of cryosections of WT and  $Pten^{Het}$  adult DRGs with specific markers (Scale 100 μm). (B) Quantification of the proportion of Isl1/2+ neurons shows no significant difference in the total population of neurons in  $Pten^{Het}$  and WT littermate DRGs (n=5, p=0.57, Wilcoxon test and Bonferroni post hoc correction). (C) Quantification of each major DRG neuronal subtype in WT and  $Pten^{Het}$  mutants. There were no significant changes in the number of Calbindin positive (CB+)  $A\beta$ -LTMRs or TrkB+  $A\delta$ -LTMRs (CB+  $A\beta$ -LTMR:  $15.3\% \pm 3.4\%$  in WT vs.  $10.8\% \pm 1.1\%$  in  $Pten^{Het}$ , n=5, p=0.293 and TrkB+  $29.2.5\% \pm 2.1\%$  in WT vs.  $22.2\% \pm 2.0\%$  in  $Pten^{Het}$ , n=5, p=0.060, Wilcoxon test and Bonferroni post hoc correction). Tyrosine hydroxylase positive (TH+) C-LTMRs are increased in  $Pten^{Het}$  mutants compared to WT littermates ( $8.8\% \pm 1.8\%$  in WT vs.  $23.8\% \pm 2.0\%$  in  $Pten^{Het}$ , n=5, p=0.0261, Wilcoxon test and Bonferroni post hoc correction). Quantification of IB4-positive non-peptidergic nociceptors shows no change in  $Pten^{Het}$  mutants compared to WT controls ( $28.2\% \pm 3.6\%$  in WT vs.  $29.4.1\% \pm 4.7\%$  in  $Pten^{Het}$ , n=5, p=0.676, Wilcoxon test and Bonferroni post hoc correction). TrkA positive peptidergic nociceptors are decreased in  $Pten^{Het}$  mutants ( $25.5\% \pm 3.1\%$  in WT vs.  $13.8\% \pm 2.7\%$  in  $Pten^{Het}$ , n=5, p=0.0367, Wilcoxon test and Bonferroni post hoc correction). TrkC positive (TrkC+) proprioceptors were increased in  $Pten^{Het}$  mutants compared to WT littermates ( $14.8\% \pm 2.4\%$  in WT vs.  $3.9\% \pm 5.6\%$  in  $Pten^{Het}$ , n=5 p=0.0122, Wilcoxon test and Bonferroni post hoc correction). \*indicate which data points are statistically significiant based on the P values.

little is known about its contribution to the in vivo development and function of peripheral somatosensory neurons in the DRG. Using a combination of behavioral analysis, transcriptional profiling, and in vivo analysis of DRG development, we have identified a critical role for *Pten* in the control of subtypespecific differentiation in primary sensory neurons. These results provide a molecular basis for developmental mechanisms

underlying the emergence of complex sensory alterations in a mouse model for syndromic ASD.

*PTEN* plays a critical role in many neurodevelopmental processes (Skelton et al. 2020). *Pten* heterozygous mouse mutants recapitulate many of the behavioral phenotypes seen in patients with ASD, including social deficits, repetitive behaviors, and

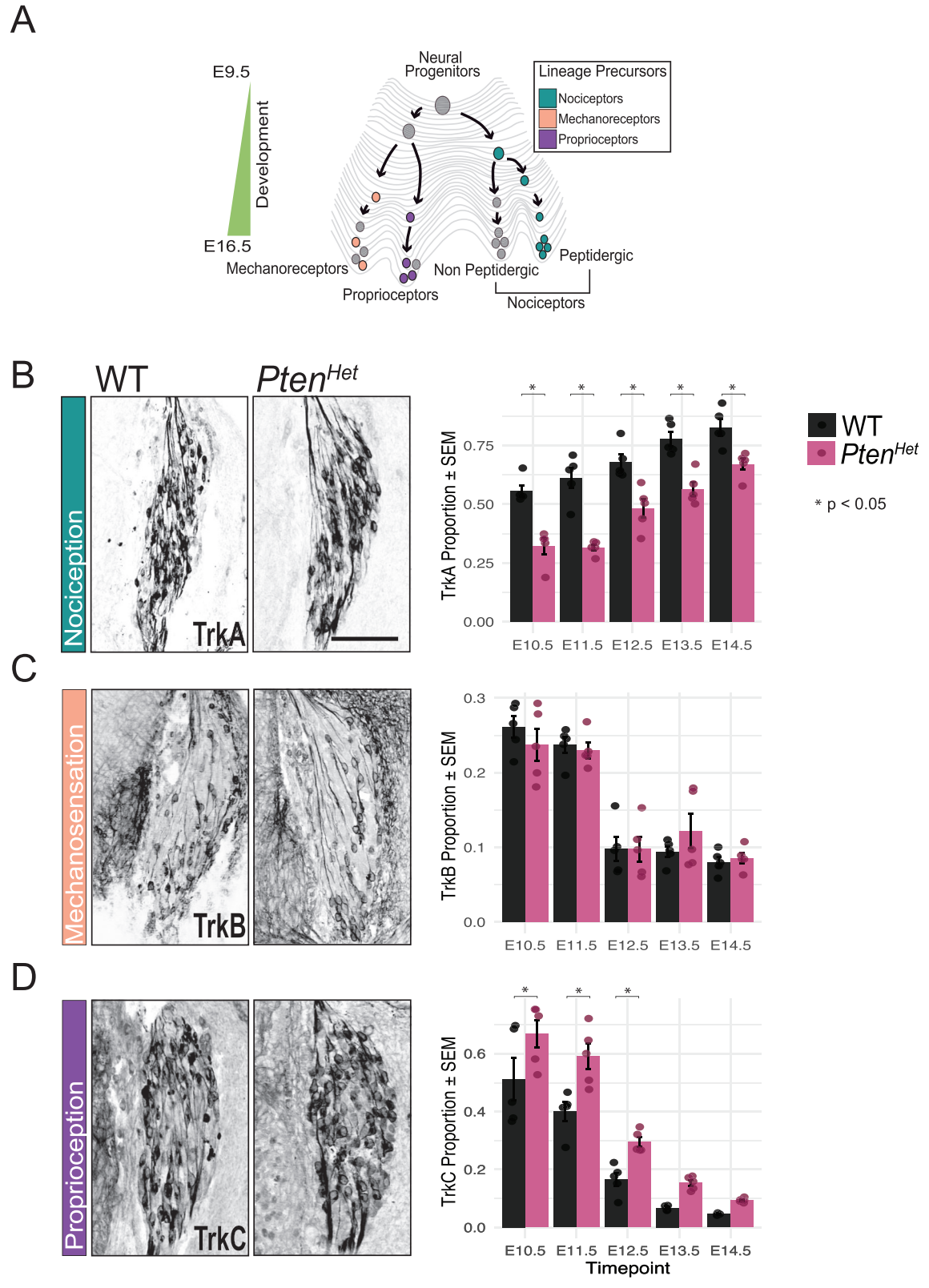


FIGURE 4 | Legend on next page.

anxiety. At the cellular level, this is accompanied by widespread brain overgrowth, altered scaling of neuronal and glial cell populations, increased axonal branching, hyperconnectivity, and decreased intrinsic excitability due to altered expression of ion channels (Chen et al. 2015; Huang et al. 2016; Clipperton-Allen and Page 2014; Garcia-Junco-Clemente et al. 2013). These

results indicate multiple distinct mechanisms underlying the complexity of behavioral phenotypes in *Pten* heterozygous models (Chen et al. 2015; Garcia-Junco-Clemente et al. 2013).

A recent transcriptomic analysis revealed that during cortical development, heterozygous deletion of *Pten* affects downstream

**FIGURE 4** | Neuronal differentiation is altered in  $Pten^{Het}$  mutants early in development. (A) Illustration of developmental landscape showing progression of DRG neuron diversification. (B–D) Representative images of cryosections of WT and  $Pten^{Het}$  E11.5 DRGs with markers of each subtype (left panels) and quantification (right panels) (Scale  $100\,\mu\text{m}$ ). (B) Representative images of DRGs labeled with TrkA (left), quantification (right) (n=5, E10.5–E13.5: p<0.001, E14.5: p<0.002, 2-way ANOVA followed by Tukey's HSD post hoc pair-wise comparisons with correction for multiple testing). (C) Images showing DRGs labeled with TrkB (left), quantification (right) shows no changes the number of TrkB+ neurons in  $Pten^{Het}$  mutants (n=5, E10.5–E14.5: p>0.05 for each timepoint, 2-way ANOVA followed by Tukey's HSD post hoc pair-wise comparisons with correction for multiple testing). (D) Images of E11.5 DRGs labeled with TrkC (left), quantification (right) shows an increase in the proportion of TrkC+ neurons in  $Pten^{Het}$  mutants compared to WT littermates between E10.5 and E12.5 but not between E13.5 and E14.5 (n=5, E10.5–E12.5: p<0.02, E13.5: p=0.08, E14.5 p=0.32 and E13.5–E14.5: p>0.05, 2-way ANOVA followed by Tukey's HSD post hoc pair-wise comparisons with correction for multiple testing). \*indicate which data points are statistically significiant based on the P values indictated in the figure legends.

signaling differently in astrocytes and neurons (Cheung et al. 2023). Our transcriptomic data (Figure 2) and in vivo analysis (Figures 3-6) provide evidence supporting a role for proper PTEN levels in DRG neuron subtype differentiation. One limitation of our study is our inability to compare PTEN protein levels in the DRG of Pten heterozygous mouse mutants and WT littermates. Recent work shows that PTEN protein is enriched in adult non-peptidergic nociceptors, suggesting that the roles of PTEN signaling vary among population subtypes (Hu et al. 2022). Our attempts to evaluate potential changes in PTEN protein levels in the DRG of PtenHet mice by immunohistochemistry and western blotting yielded ambiguous results. Future studies that account for cellular heterogeneity in DRGs will be needed for a clearer understanding of population-specific effects of Pten heterozygous deletion. Notably, we see similar defects in DRG neuron diversification in both *Pten*<sup>Het</sup> and *Pten*<sup>Y68H/+</sup> mice. Although sensory behaviors have not yet been thoroughly characterized in Pten Y68H/+ mutants, these mice exhibit autism-like phenotypes similar to those observed in PtenHet animals (Sarn et al. 2021). Based on our molecular findings, PtenY68H/+ mice are likely to recapitulate the sensory alterations seen in Pten<sup>Het</sup> models. Future studies will be necessary to determine the extent to which our results extend to this patient-specific mutation.

While antibody compatibility limited our ability to perform broad subtype co-labeling, the observed changes still reveal meaningful alterations in marker expression, subtype composition, or specification. We show that these defects arise early in development (Figure 4) and engage canonical pathways downstream of PTEN (Figure 5). This is supported by the observation that both TSC/mTOR and GSK-3β/β-Catenin signaling pathways are dysregulated in PtenHet DRGs. Interestingly, these pathways seem to be specifically regulated in different DRG populations. In PtenHet mutants, both mTOR and GSK--3β/β-Catenin pathways are hyperactive in TrkC<sup>+</sup> DRG neurons in Pten<sup>Het</sup> mutants, whereas only pS6 was significantly elevated in TrkA+ DRG neurons and both pathways appeared normal in TrkB<sup>+</sup> DRG neurons. Why some cell types are more sensitive to Pten gene dosage than others remains a subject of current investigation. This could reflect intrinsic differences in how signaling pathways downstream of specific Trk receptors are regulated.

Similar patterns of cell-type-specific vulnerability have been observed in the central nervous system, with reduced *Pten* dosage not only increasing cell growth and dendritic complexity, but also interfering with temporal coordination of terminal differentiation and establishment of functional synaptic connectivity (Chen et al. 2015). In our study, the differential sensitivity

of DRG subtypes to Pten loss may reflect analogous signaling imbalances during sensory neurogenesis. The selective hyperactivation of mTOR and GSK-3β/β-catenin in TrkC+ neurons, and the more limited pS6 elevation in TrkA+ populations, suggest that each sensory lineage integrates PTEN-regulated pathways through distinct molecular logic. This may impact not only cell size and survival, but also the transcriptional programs required for maturation and synapse formation (Tilot et al. 2015). Given the tightly choreographed timeline of DRG subtype specification and target innervation, even modest shifts in signaling could desynchronize developmental checkpoints, resulting in neurons that express marker genes inappropriately or fail to form precise connections. From a broader perspective, these findings support the emerging view that PTEN-associated ASD arises not solely from circuit overgrowth or synaptic excess, but from a failure to properly regulate cell fate, timing, and connectivity across neural systems.

One limitation of the current study is that we did not directly examine the electrophysiological function of DRG subtypes in Pten<sup>Het</sup> mutants. However, the somatosensory behavioral phenotypes observed in PtenHet mutants offer insights into the consequences of developmental disruptions mediated by altered PTEN signaling. Increased "wet-dog shake" behaviors in Pten<sup>Het</sup> mutants (Figure 1F) may reflect changes in sensory neuron populations, potentially influenced by increased density or ectopic expression of TH-positive C-LTMR markers (Figure 3), leading to heightened tactile sensitivity. Similarly, sensorimotor impairments (Figure 1B,C) could result from functional alterations in proprioceptive neurons, possibly arising from ectopic or dysregulated TrkC expression patterns (Figure 3) affecting sensorimotor feedback loops critical for coordination (Akay et al. 2014; Inacio et al. 2016). A recent study has demonstrated that neuron-specific Pten deletion using Nse-Cre leads to impaired cerebellar-dependent motor learning and disrupted intracellular signaling, particularly involving hyperactive mTOR and altered GSK3β activity (Nolan et al. 2019). These results support the idea that disrupted PTEN-regulated pathways affect sensorimotor integration not only at the level of peripheral sensory neurons but also in central motor learning circuits, reinforcing a systems-level contribution to the observed behavioral deficits.

In contrast, the relationship between reduced thermal sensitivity and the altered representation of TrkA-positive neurons remains uncertain. Recent evidence of abnormal itch and thermal sensitivity resulting from ectopic expression of *TRPV1* and *MrgprA3* in non-peptidergic neurons following adult-specific *Pten* deletion further highlights the complexity of subtype-specific

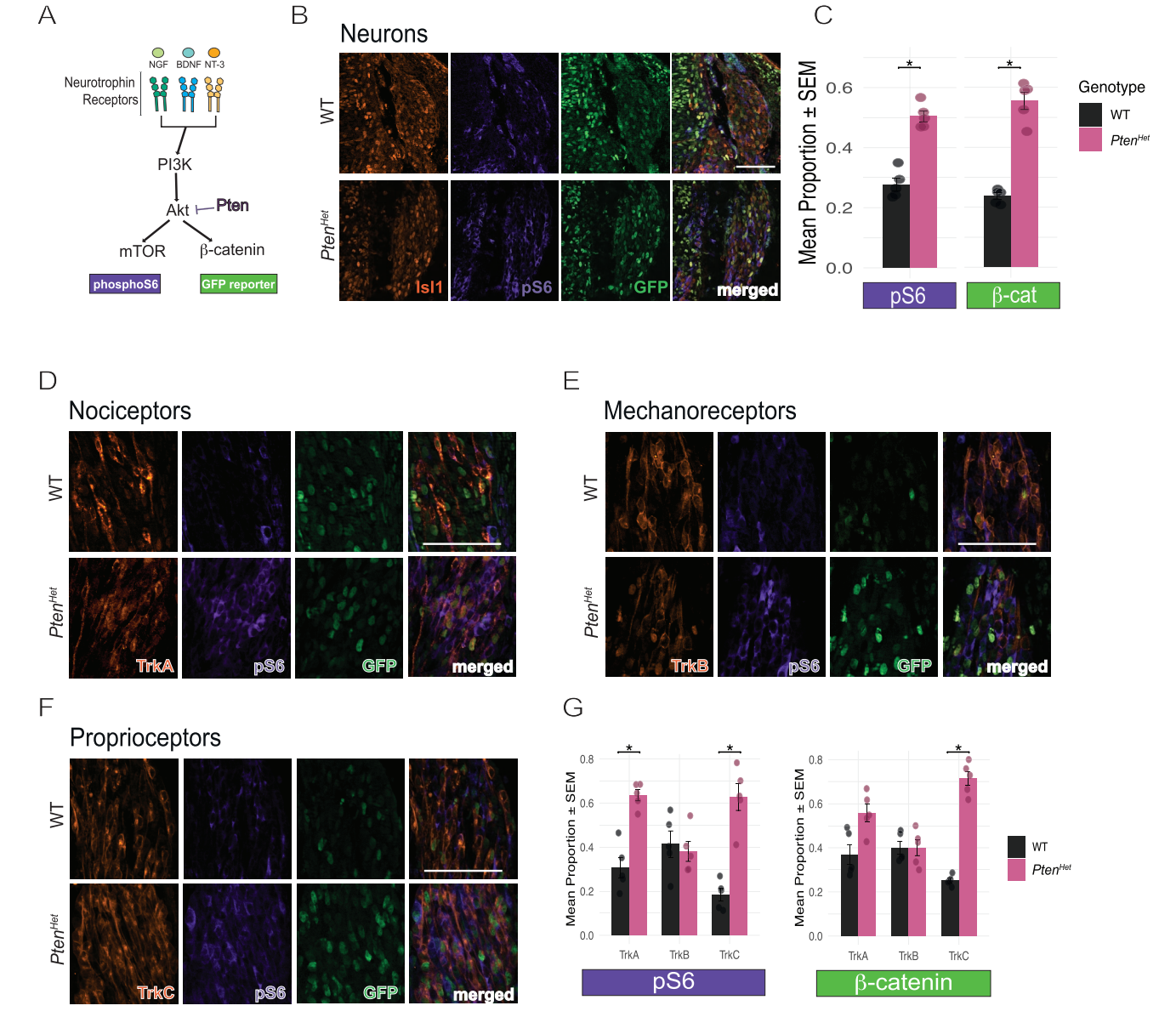
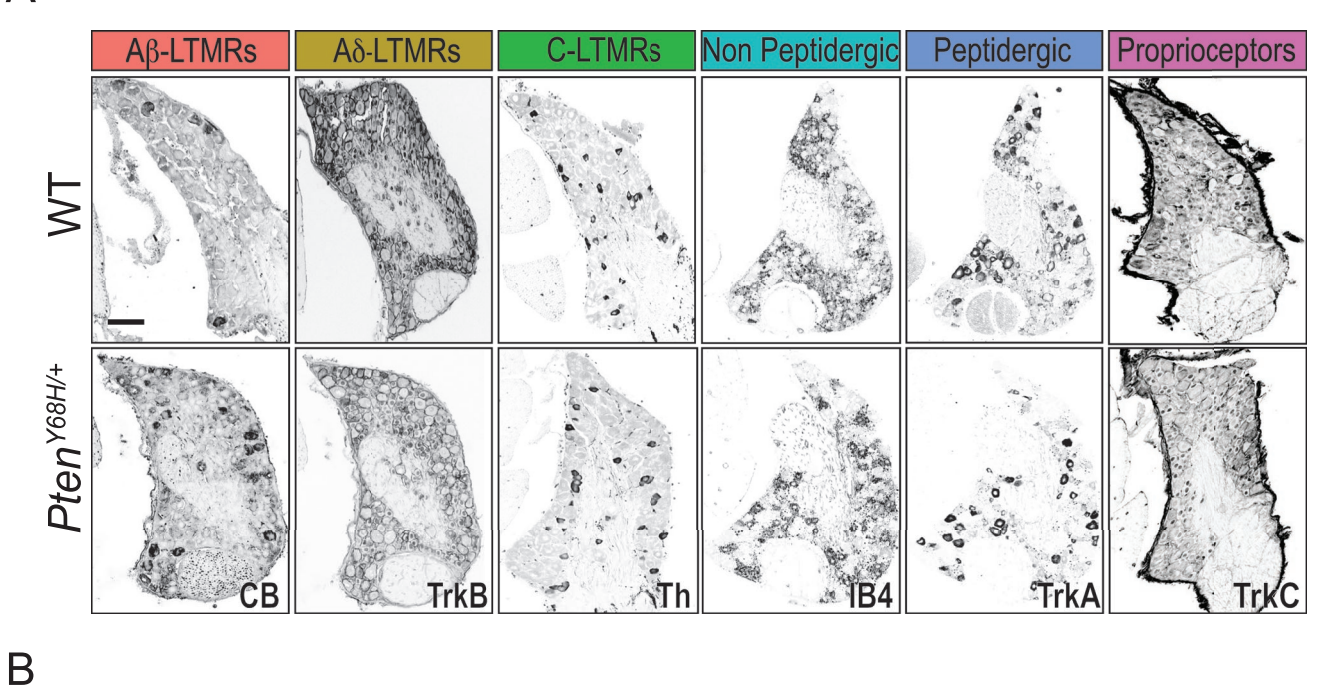


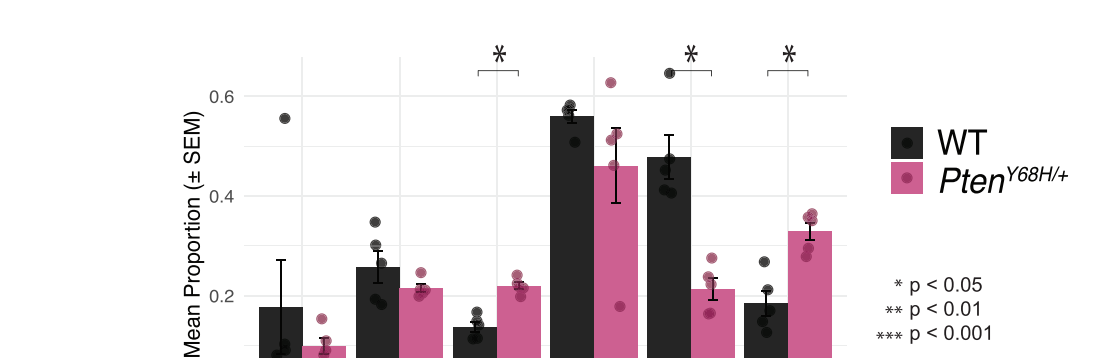
FIGURE 5 | Pten haploinsufficiency alters signaling downstream of PI3K/AKT in TrkA and TrkC lineages. (A) Schematic representation of mTOR and GSK-3β signaling pathways downstream of Trk receptor activation of PI3K/AKT. (B, D-F) Representative images of E11.5 DRGs of WT and PtenHet littermates immunolabeled with Isl1 (B), TrkA (D), TrkB (E), TrkC (F) (orange), phospho-S6 (pS6) (purple) and GFP (green) to measure activity of the mTOR and GSK-3β/β-catenin pathways, respectively (Scale 100 μm). (C) Quantification of Isl1+ neurons positive for activation of pS6 (left) and  $\beta$ -catenin ( $\beta$ -cat, right) in E11.5 DRGs from WT and  $Pten^{Het}$  mice. There was an increase in the proportion of pS6<sup>+</sup>/Isl1<sup>+</sup> neurons in  $Pten^{Het}$ compared to WT (27.7%  $\pm$  2.0% in WT vs. 50.4%  $\pm$  1.8% in  $Pten^{Het}$ , n = 5, p < 0.041, Wilcoxon test and Bonferroni post hoc correction). The proportion of GFP+/Isl1+ neurons was also increased in mutants compared to controls  $(23.7\% \pm 1.0\%$  in WT vs.  $55.5 \pm 2.9$  in  $Pten^{Het}, n = 5, p < 0.031$ , Wilcoxon test and Bonferroni post hoc correction). (G) Quantification of pS6 (left) and GFP (right) positive neurons within each DRG neuron subtype. Within the  $TrkA\ population, the\ pS6^+/TrkA^+\ neurons\ were\ increased\ in\ \textit{Pten}^{\textit{Het}}, compared\ to\ WT\ littermates\ (left,\ 30.5\%\,\pm\,4.7\%\ in\ WT\ vs.\ 63.4\,\pm\,5.4\ in\ \textit{Pten}^{\textit{Het}}, compared\ to\ WT\ littermates\ (left,\ 30.5\%\,\pm\,4.7\%\ in\ WT\ vs.\ 63.4\,\pm\,5.4\ in\ \textit{Pten}^{\textit{Het}}, compared\ to\ WT\ littermates\ (left,\ 30.5\%\,\pm\,4.7\%\ in\ WT\ vs.\ 63.4\,\pm\,5.4\ in\ \textit{Pten}^{\textit{Het}}, compared\ to\ WT\ littermates\ (left,\ 30.5\%\,\pm\,4.7\%\ in\ WT\ vs.\ 63.4\,\pm\,5.4\ in\ \textit{Pten}^{\textit{Het}}, compared\ to\ WT\ littermates\ (left,\ 30.5\%\,\pm\,4.7\%\ in\ WT\ vs.\ 63.4\,\pm\,5.4\ in\ \textit{Pten}^{\textit{Het}}, compared\ to\ WT\ littermates\ (left,\ 30.5\%\,\pm\,4.7\%\ in\ WT\ vs.\ 63.4\,\pm\,5.4\ in\ \textit{Pten}^{\textit{Het}}, compared\ to\ WT\ littermates\ (left,\ 30.5\%\,\pm\,4.7\%\ in\ WT\ vs.\ 63.4\,\pm\,5.4\ in\ \textit{Pten}^{\textit{Het}}, compared\ to\ WT\ littermates\ (left,\ 30.5\%\,\pm\,4.7\%\ in\ WT\ vs.\ 63.4\,\pm\,5.4\ in\ \textit{Pten}^{\textit{Het}}, compared\ to\ WT\ littermates\ (left,\ 30.5\%\,\pm\,4.7\%\ in\ WT\ vs.\ 63.4\,\pm\,5.4\ in\ \textit{Pten}^{\textit{Het}}, compared\ to\ WT\ littermates\ (left,\ 30.5\%\,\pm\,4.7\%\ in\ WT\ vs.\ 63.4\,\pm\,5.4\ in\ \textit{Pten}^{\textit{Het}}, compared\ to\ WT\ littermates\ (left,\ 30.5\%\,\pm\,4.7\%\ in\ WT\ vs.\ 63.4\,\pm\,5.4\ in\ \textit{Pten}^{\textit{Het}}, compared\ to\ WT\ littermates\ (left,\ 30.5\%\,\pm\,4.7\%\ in\ WT\ vs.\ 63.4\,\pm\,5.4\ in\ \textit{Pten}^{\textit{Het}}, compared\ to\ WT\ littermates\ (left,\ 30.5\%\,\pm\,4.7\%\ in\ WT\ vs.\ 63.4\,\pm\,5.4\ in\ WT\ littermates\ (left,\ 30.5\%\,\pm\,4.7\%\ in\ WT\ vs.\ 63.4\,\pm\,5.4\ in\ WT\ littermates\ (left,\ 30.5\%\,\pm\,5.4\ in\ WT\ vs.\ 63.4\,\pm\,5.4\ in\ WT\ littermates\ (left,\ 30.5\%\,\pm\,5.4\ in\ WT\ vs.\ 63.4\,\pm\,5.4\ in\ WT\ littermates\ (left,\ 30.5\%\,\pm\,5.4\ in\ WT\ vs.\ 63.4\,\pm\,5.4\ in\ WT\ littermates\ (left,\ 30.5\%\,\pm\,5.4\ in\ WT\ littermates\ (left,\ 30.5\%$ n=5, p<0.031, Wilcoxon test and Bonferroni post hoc correction), while there was no significant change in the number of GFP<sup>+</sup>/TrkA<sup>+</sup> neurons  $(36.8\% \pm 5.4\%)$  in WT vs.  $54.4 \pm 4.0$  in  $Pten^{Het}$ , n = 5, p = 0.12, Wilcoxon test and Bonferroni post hoc correction). Quantification in TrkB<sup>+</sup> neurons shows no significant change in the proportions of pS6+/TrkB+ neurons between  $Pten^{Het}$  and WT controls (41.3%  $\pm$  5.9% in WT vs. 38.0  $\pm$  4.5 in  $Pten^{Het}$ , n = 5, p = 0.99, Wilcoxon test and Bonferroni post hoc correction) or in the proportion of GFP<sup>+</sup>/TrkB<sup>+</sup> neurons (39.9%  $\pm$  2.9% in WT vs. 40.0  $\pm$  3.6 in  $Pten^{Het}$ , n = 5, p = 0.99, Wilcoxon test and Bonferroni post hoc correction). There was an increased number of pS6+/TrkC+ neurons in  $Pten^{Het}$  compared to WT littermates ( $18.4\% \pm 2.5\%$  in WT vs.  $62.8 \pm 6.1$  in  $Pten^{Het}$ , n = 5, p = 0.031, Wilcoxon test and Bonferroni post hoc correction, left), and GFP+/TrkC+ neurons in  $Pten^{Het}$  compared to controls (25.1%  $\pm$  1.0% in WT vs. 71.4  $\pm$  3.2 in  $Pten^{Het}$ , n = 5, p = 0.0031, Wilcoxon test and Bonferroni post hoc correction). \*indicate which data points are statistically significiant based on the P values indictaed in the figure legends.

marker expression and sensory neuron functionality. (Hu et al. 2022). Whether the altered expression profiles observed in adult  $Pten^{Het}$  DRGs arise predominantly from shifts in subtype

populations, ectopic marker expression, or reduced specificity of neuronal subtype markers remains to be clarified. The coexistence of tactile hypersensitivity and thermal hyposensitivity







IB4

FIGURE 6 | DRG neuron diversification is abnormal in PtenY68H/+ mice. (A) Representative images of cryosections from WT (top) and PtenY68H/+ (bottom) P21 DRGs labeled with specific markers for select DRG subtypes (Scale 100 µm). (B) Quantification shows subtype-specific alterations in DRG neurons in  $Pten^{Y68H/+}$  compared to WT littermates. The proportions of CB<sup>+</sup> A $\beta$ -LTMRs and TrkB<sup>+</sup> A $\delta$ -LTMR were unchanged in  $Pten^{Y68H/+}$ mutants, while there was a significant increase in the proportion of TH<sup>+</sup> C-LTMRs (CB1:  $17.5\% \pm 9.4\%$  in WT vs.  $9.4\% \pm 1.5\%$  in  $Pten^{Y68H/+}$ , n=5, p = 0.99; TrkB:  $25.5\% \pm 3.1\%$  in WT vs.  $21.5\% \pm 0.8\%$  in  $Pten^{Y68H/+}$ , n = 5, p = 0.676, Wilcoxon test and Bonferroni post hoc correction; TH:  $13.7\% \pm 1.0\%$ in WT vs. 21.9% ±0.7% in Pten Y68H/+, n = 5, p = 0.0122, Wilcoxon test and Bonferroni post hoc correction). There were no changes in the proportion of IB4+ non-peptidergic nociceptors and a significant decrease in the proportion of TrkA+ peptidergic nociceptors in PtenY68H/+ when compared to littermate controls (56.0%  $\pm$  1.3% in WT vs. 46.1%  $\pm$  7.5% in  $Pten^{Y68H/+}$ , n = 5, p = 0.296; TrkA: 47.8%  $\pm$  4.3% in WT vs. 21.3%  $\pm$  2.1% in  $Pten^{Y68H/+}$ , n = 5, p = 0.296; TrkA: 47.8%  $\pm$  4.3% in WT vs. 21.3%  $\pm$  2.1% in  $Pten^{Y68H/+}$ , n = 5, p = 0.296; TrkA: 47.8%  $\pm$  4.3% in WT vs. 21.3%  $\pm$  2.1% in  $Pten^{Y68H/+}$ , n = 5, p = 0.296; TrkA: 47.8%  $\pm$  4.3% in WT vs. 21.3%  $\pm$  2.1% in  $Pten^{Y68H/+}$ , n = 5, p = 0.296; TrkA: 47.8%  $\pm$  4.3% in WT vs. 21.3%  $\pm$  2.1% in  $Pten^{Y68H/+}$ , n = 5, p = 0.296; TrkA: 47.8%  $\pm$  4.3% in WT vs. 21.3%  $\pm$  2.1% in  $Pten^{Y68H/+}$ , n = 5, p = 0.296; TrkA: 47.8%  $\pm$  4.3% in WT vs. 21.3%  $\pm$  2.1% in  $Pten^{Y68H/+}$ , n = 5, p = 0.296; TrkA: 47.8%  $\pm$  4.3% in  $Pten^{Y68H/+}$ , p = 5, p = 0.296; TrkA: 47.8%  $\pm$  4.3% in  $Pten^{Y68H/+}$ , p = 5, p = 0.296; TrkA: 47.8%  $\pm$  4.3% in  $Pten^{Y68H/+}$ , p = 5, p = 0.296; TrkA: 47.8%  $\pm$  4.3% in  $Pten^{Y68H/+}$ , p = 5, p = 0.296; p = 0.2p = 0.0122, Wilcoxon test and Bonferroni post hoc correction). There was a significant increase in the proportion of TrkC<sup>+</sup> neurons in  $Pten^{Y68H/+}$  mutants compared to WT littermate controls (18.5%  $\pm$  2.5% in WT vs. 32.9%  $\pm$  1.7% in  $Pten^{Y68H/+}$ , n = 5 p = 0.0122, Wilcoxon test and Bonferroni post hoc correction). \*indicate which data points are statistically signficiant based on the P values indictaed in the figure legends.

TrkA

in PtenHet mice, moreover, parallels the sensory heterogeneity often reported in individuals with ASD (Baranek et al. 2006), suggesting that these divergent phenotypes may arise from distinct underlying circuit mechanisms. Further electrophysiological studies will be essential to determine whether these behavioral alterations reflect changes in the excitability of specific DRG subtypes or broader dysfunctions in sensory processing pathways. Nevertheless, embryonic analyses indicating early disruptions in TrkA and TrkC lineage differentiation suggest

0.0

that early developmental changes contribute to functional sensory alterations observed in adulthood.

p < 0.001

Our findings align with emerging evidence highlighting sensory circuit alterations in rodent models carrying mutations in ASD-susceptibility genes (Orefice et al. 2016, 2019; Price and Melemedjian 2012; He et al. 2017; Chelini et al. 2019; Deng et al. 2021; Han et al. 2016; Dawes et al. 2018). Rats with mutations in Mecp2 exhibit abnormal mechanical and thermal sensitivity

linked to abnormal sensory neuron postnatal development and function (Bhattacherjee, Mu, et al. 2017). Moreover, selective deletion of Mecp2 or Gabrb3 in somatosensory neurons results in tactile sensory defects, social impairments, and anxietylike behaviors, further establishing sensory dysfunction as an integral aspect of ASD pathophysiology (Orefice et al. 2016). Interestingly, the developmental timing of somatosensory defects aligns closely with the onset of ASD-like behaviors, reinforcing a developmental origin for sensory abnormalities in ASD models (Tasnim et al. 2024). Pharmacologically reducing tactile overactivity in Mecp2 and Shank3 mutants has demonstrated potential in alleviating anxiety-like behaviors and social deficits, highlighting sensory dysfunction as a tractable therapeutic target (Orefice et al. 2019). Tactile sensory processing deficits appear to be conserved across multiple genetic mouse models of ASD, further supporting the view that peripheral somatosensory dysfunction is a common and early-emerging feature of ASD pathophysiology (Falcao et al. 2024). This perspective is also reinforced by clinical and preclinical insights: Tactile hypersensitivity and hyposensitivity are not only frequently reported in individuals with ASD, but are also replicated across diverse rodent models, reflecting a translationally conserved somatosensory phenotype (Balasco et al. 2019). Given that atypical sensory sensitivities affect approximately 90% of individuals with ASD (Ben-Sasson et al. 2009), further elucidation of the molecular and cellular underpinnings of these sensory phenotypes is essential to advance therapeutic interventions.

#### Acknowledgments

We would like to thank the members of the Wright laboratory for their assistance and discussion throughout the course of this study. Special thanks to Dr. Matthew Pomaville for his insight and help with experimental troubleshooting. We also thank Dr. Martin Riccomagno, Dr. Brian O'Roak, and Dr. Arpiar Saunders for their helpful suggestions on the manuscript. This work was supported by NIH grant R01NS091027 (K.M.W.), OHSU Fellowship for Diversity in Research (A.F.), Collins Medical Trust (A.F.) and NIH grant K01NS116168 (A.F.). C.E. passed away during the preparation of this manuscript and was the Sondra J and Stephen R Hardis Chair of Cancer Genomic Medicine at the Cleveland Clinic and thanks the Ambrose Monell Foundation.

#### **Conflicts of Interest**

The authors declare no conflicts of interest.

#### **Data Availability Statement**

The data that support the findings of this study are available from the corresponding author upon reasonable request.

#### References

Abraira, V. E., and D. D. Ginty. 2013. "The Sensory Neurons of Touch." *Neuron* 79, no. 4: 618–639.

Akay, T., W. G. Tourtellotte, S. Arber, and T. M. Jessell. 2014. "Degradation of Mouse Locomotor Pattern in the Absence of Proprioceptive Sensory Feedback." *Proceedings of the National Academy of Sciences of the United States of America* 111, no. 47: 16877–16882.

Aksamitiene, E., A. Kiyatkin, and B. N. Kholodenko. 2012. "Cross-Talk Between Mitogenic Ras/MAPK and Survival PI3K/Akt

Pathways: A Fine Balance." *Biochemical Society Transactions* 40, no. 1: 139–146.

Arber, S., D. R. Ladle, J. H. Lin, E. Frank, and T. M. Jessell. 2000. "ETS Gene Er81 Controls the Formation of Functional Connections Between Group Ia Sensory Afferents and Motor Neurons." *Cell* 101, no. 5: 485–498.

Arcourt, A., L. Gorham, R. Dhandapani, et al. 2017. "Touch Receptor-Derived Sensory Information Alleviates Acute Pain Signaling and Fine-Tunes Nociceptive Reflex Coordination." *Neuron* 93, no. 1: 179–193.

Bai, L., B. P. Lehnert, J. Liu, et al. 2015. "Genetic Identification of an Expansive Mechanoreceptor Sensitive to Skin Stroking." *Cell* 163, no. 7: 1783–1795.

Balasco, L., G. Provenzano, and Y. Bozzi. 2019. "Sensory Abnormalities in Autism Spectrum Disorders: A Focus on the Tactile Domain, From Genetic Mouse Models to the Clinic." *Frontiers in Psychiatry* 10: 1016.

Baranek, G. T., F. J. David, M. D. Poe, W. L. Stone, and L. R. Watson. 2006. "Sensory Experiences Questionnaire: Discriminating Sensory Features in Young Children With Autism, Developmental Delays, and Typical Development." *Journal of Child Psychology and Psychiatry* 47, no. 6: 591–601.

Basbaum, A. I., D. M. Bautista, G. Scherrer, and D. Julius. 2009. "Cellular and Molecular Mechanisms of Pain." *Cell* 139, no. 2: 267–284.

Belkaid, Y., and J. A. Segre. 2014. "Dialogue Between Skin Microbiota and Immunity." *Science* 346, no. 6212: 954–959.

Ben-Sasson, A., L. Hen, R. Fluss, S. A. Cermak, B. Engel-Yeger, and E. Gal. 2009. "A Meta-Analysis of Sensory Modulation Symptoms in Individuals With Autism Spectrum Disorders." *Journal of Autism and Developmental Disorders* 39, no. 1: 1–11.

Bhattacherjee, A., Y. Mu, M. K. Winter, et al. 2017. "Neuronal Cytoskeletal Gene Dysregulation and Mechanical Hypersensitivity in a Rat Model of Rett Syndrome." *Proceedings of the National Academy of Sciences of the United States of America* 114, no. 33: E6952–E6961.

Bhattacherjee, A., M. Winter, L. Eggimann, et al. 2017. "Motor, Somatosensory, Viscerosensory and Metabolic Impairments in a Heterozygous Female Rat Model of Rett Syndrome." *International Journal of Molecular Sciences* 19, no. 1: 97.

Bouet, V., M. Boulouard, J. Toutain, et al. 2009. "The Adhesive Removal Test: A Sensitive Method to Assess Sensorimotor Deficits in Mice." *Nature Protocols* 4, no. 10: 1560–1564.

Busa, T., B. Chabrol, O. Perret, M. Longy, and N. Philip. 2013. "Novel PTEN Germline Mutation in a Family With Mild Phenotype: Difficulties in Genetic Counseling." *Gene* 512, no. 2: 194–197.

Busch, R. M., S. Srivastava, O. Hogue, et al. 2019. "Neurobehavioral Phenotype of Autism Spectrum Disorder Associated With Germline Heterozygous Mutations in PTEN." *Translational Psychiatry* 9, no. 1: 253.

Cascio, C. J. 2010. "Somatosensory Processing in Neurodevelopmental Disorders." *Journal of Neurodevelopmental Disorders* 2, no. 2: 62–69.

Cavanaugh, D. J., H. Lee, L. Lo, et al. 2009. "Distinct Subsets of Unmyelinated Primary Sensory Fibers Mediate Behavioral Responses to Noxious Thermal and Mechanical Stimuli." *Proceedings of the National Academy of Sciences of the United States of America* 106, no. 22: 9075–9080.

Chelini, G., V. Zerbi, L. Cimino, et al. 2019. "Aberrant Somatosensory Processing and Connectivity in Mice Lacking Engrailed-2." *Journal of Neuroscience* 39, no. 8: 1525–1538.

Chen, Y., W. C. Huang, J. Sejourne, A. E. Clipperton-Allen, and D. T. Page. 2015. "Pten Mutations Alter Brain Growth Trajectory and

- Allocation of Cell Types Through Elevated Beta-Catenin Signaling." *Journal of Neuroscience* 35, no. 28: 10252–10267.
- Cheung, S. K. K., J. Kwok, P. M. Y. Or, et al. 2023. "Neuropathological Signatures Revealed by Transcriptomic and Proteomic Analysis in Pten-Deficient Mouse Models." *Scientific Reports* 13, no. 1: 6763.
- Clipperton-Allen, A. E., and D. T. Page. 2014. "Pten Haploinsufficient Mice Show Broad Brain Overgrowth but Selective Impairments in Autism-Relevant Behavioral Tests." *Human Molecular Genetics* 23, no. 13: 3490–3505.
- Clipperton-Allen, A. E., and D. T. Page. 2020. "Connecting Genotype With Behavioral Phenotype in Mouse Models of Autism Associated With PTEN Mutations." *Cold Spring Harbor Perspectives in Medicine* 10, no. 9: a037010.
- Clipperton-Allen, A. E., H. Swick, V. Botero, et al. 2022. "Pten Haploinsufficiency Causes Desynchronized Growth of Brain Areas Involved in Sensory Processing." *iScience* 25, no. 2: 103796.
- Crino, P. B., K. L. Nathanson, and E. P. Henske. 2006. "The Tuberous Sclerosis Complex." *New England Journal of Medicine* 355, no. 13: 1345–1356.
- Crowley, C., S. D. Spencer, M. C. Nishimura, et al. 1994. "Mice Lacking Nerve Growth Factor Display Perinatal Loss of Sensory and Sympathetic Neurons Yet Develop Basal Forebrain Cholinergic Neurons." *Cell* 76, no. 6: 1001–1011.
- Datta, S. R., H. Dudek, X. Tao, et al. 1997. "Akt Phosphorylation of BAD Couples Survival Signals to the Cell-Intrinsic Death Machinery." *Cell* 91, no. 2: 231–241.
- Dawes, J. M., G. A. Weir, S. J. Middleton, et al. 2018. "Immune or Genetic-Mediated Disruption of CASPR2 Causes Pain Hypersensitivity due to Enhanced Primary Afferent Excitability." *Neuron* 97, no. 4: 806–822.
- DeLorey, T. M., P. Sahbaie, E. Hashemi, W. W. Li, A. Salehi, and D. J. Clark. 2011. "Somatosensory and Sensorimotor Consequences Associated With the Heterozygous Disruption of the Autism Candidate Gene, Gabrb3." *Behavioural Brain Research* 216, no. 1: 36–45.
- Deng, P. Y., O. Avraham, V. Cavalli, and V. A. Klyachko. 2021. "Hyperexcitability of Sensory Neurons in Fragile X Mouse Model." *Frontiers in Molecular Neuroscience* 14: 796053.
- Falcao, M., P. Monteiro, and L. Jacinto. 2024. "Tactile Sensory Processing Deficits in Genetic Mouse Models of Autism Spectrum Disorder." *Journal of Neurochemistry* 168, no. 9: 2105–2123.
- Ferrer-Vaquer, A., A. Piliszek, G. Tian, R. J. Aho, D. Dufort, and A. K. Hadjantonakis. 2010. "A Sensitive and Bright Single-Cell Resolution Live Imaging Reporter of Wnt/Ss-Catenin Signaling in the Mouse." *BMC Developmental Biology* 10: 121.
- Frazier, T. W. 2019. "Autism Spectrum Disorder Associated With Germline Heterozygous PTEN Mutations." *Cold Spring Harbor Perspectives in Medicine* 9, no. 10: a037002.
- Garcia-Junco-Clemente, P., D. K. Chow, E. Tring, M. T. Lazaro, J. T. Trachtenberg, and P. Golshani. 2013. "Overexpression of Calcium-Activated Potassium Channels Underlies Cortical Dysfunction in a Model of PTEN-Associated Autism." Proceedings of the National Academy of Sciences of the United States of America 110, no. 45: 18297–18302.
- Georgescu, M. M. 2010. "PTEN Tumor Suppressor Network in PI3K-Akt Pathway Control." Genes & Cancer 1, no. 12: 1170–1177.
- Ghitani, N., A. Barik, M. Szczot, et al. 2017. "Specialized Mechanosensory Nociceptors Mediating Rapid Responses to Hair Pull." *Neuron* 95, no. 4: 944–954.
- Gutierrez, G. C., S. L. Smalley, and P. E. Tanguay. 1998. "Autism in Tuberous Sclerosis Complex." *Journal of Autism and Developmental Disorders* 28, no. 2: 97–103.

- Gynter, A., D. Meistermann, H. Lahdesmaki, and H. Kilpinen. 2023. "DeconV: Probabilistic Cell Type Deconvolution From Bulk RNA-Sequencing Data." *bioRxiv*. https://doi.org/10.1101/2023.12.07. 570524.
- Han, Q., Y. H. Kim, X. Wang, et al. 2016. "SHANK3 Deficiency Impairs Heat Hyperalgesia and TRPV1 Signaling in Primary Sensory Neurons." *Neuron* 92, no. 6: 1279–1293.
- Han, S. Y., H. Kato, S. Kato, et al. 2000. "Functional Evaluation of PTEN Missense Mutations Using in Vitro Phosphoinositide Phosphatase Assay." *Cancer Research* 60, no. 12: 3147–3151.
- Hansen-Kiss, E., S. Beinkampen, B. Adler, et al. 2017. "A Retrospective Chart Review of the Features of PTEN Hamartoma Tumour Syndrome in Children." *Journal of Medical Genetics* 54, no. 7: 471–478.
- He, C. X., D. A. Cantu, S. S. Mantri, W. A. Zeiger, A. Goel, and C. Portera-Cailliau. 2017. "Tactile Defensiveness and Impaired Adaptation of Neuronal Activity in the Fmr1 Knock-Out Mouse Model of Autism." *Journal of Neuroscience* 37, no. 27: 6475–6487.
- He, X., Y. Ni, Y. Wang, T. Romigh, and C. Eng. 2011. "Naturally Occurring Germline and Tumor-Associated Mutations Within the ATP-Binding Motifs of PTEN Lead to Oxidative Damage of DNA Associated With Decreased Nuclear p53." *Human Molecular Genetics* 20, no. 1: 80–89.
- Hu, L., G. Y. Jiang, Y. P. Wang, et al. 2022. "The Role of PTEN in Primary Sensory Neurons in Processing Itch and Thermal Information in Mice." *Cell Reports* 39, no. 3: 110724.
- Huang, E. J., and L. F. Reichardt. 2001. "Neurotrophins: Roles in Neuronal Development and Function." *Annual Review of Neuroscience* 24: 677–736.
- Huang, E. J., and L. F. Reichardt. 2003. "Trk Receptors: Roles in Neuronal Signal Transduction." *Annual Review of Biochemistry* 72: 609–642.
- Huang, W., H. Y. Chang, T. Fei, H. Wu, and Y. G. Chen. 2007. "GSK3 Beta Mediates Suppression of Cyclin D2 Expression by Tumor Suppressor PTEN." *Oncogene* 26, no. 17: 2471–2482.
- Huang, W. C., Y. Chen, and D. T. Page. 2016. "Hyperconnectivity of Prefrontal Cortex to Amygdala Projections in a Mouse Model of Macrocephaly/Autism Syndrome." *Nature Communications* 7: 13421.
- Huzard, D., G. Oliva, M. Marias, et al. 2024. "Primary Sensory Neuron Dysfunction Underlying Mechanical Itch Hypersensitivity in a Shank3 Mouse Model of Autism." *Translational Psychiatry* 15, no. 1: 259.
- Inacio, A. R., A. Nasretdinov, J. Lebedeva, and R. Khazipov. 2016. "Sensory Feedback Synchronizes Motor and Sensory Neuronal Networks in the Neonatal Rat Spinal Cord." *Nature Communications* 7: 13060.
- Keeler, A. B., A. L. van Deusen, I. C. Gadani, et al. 2022. "A Developmental Atlas of Somatosensory Diversification and Maturation in the Dorsal Root Ganglia by Single-Cell Mass Cytometry." *Nature Neuroscience* 25, no. 11: 1543–1558.
- Klesse, L. J., and L. F. Parada. 1998. "p21 Ras and Phosphatidylinositol-3 Kinase Are Required for Survival of Wild-Type and NF1 Mutant Sensory Neurons." *Journal of Neuroscience* 18, no. 24: 10420–10428.
- Landy, M. A., M. Goyal, and H. C. Lai. 2021. "Nociceptor Subtypes Are Born Continuously Over DRG Development." *Developmental Biology* 479: 91–98.
- Li, C. L., K. C. Li, D. Wu, et al. 2016. "Somatosensory Neuron Types Identified by High-Coverage Single-Cell RNA-Sequencing and Functional Heterogeneity." *Cell Research* 26, no. 1: 83–102.
- Li, L., M. Rutlin, V. E. Abraira, et al. 2011. "The Functional Organization of Cutaneous Low-Threshold Mechanosensory Neurons." *Cell* 147, no. 7: 1615–1627.

- Liu, D., S. P. MacFarland, L. Yehia, et al. 2024. "A Bi-Institutional Study of Gastrointestinal and Hepatic Manifestations in Children With PTEN Hamartoma Tumor Syndrome." *Gastro Hep Advances* 3, no. 2: 250–259.
- Lobo, G. P., K. A. Waite, S. M. Planchon, T. Romigh, N. T. Nassif, and C. Eng. 2009. "Germline and Somatic Cancer-Associated Mutations in the ATP-Binding Motifs of PTEN Influence Its Subcellular Localization and Tumor Suppressive Function." *Human Molecular Genetics* 18, no. 15: 2851–2862.
- Ma, Q., C. Fode, F. Guillemot, and D. J. Anderson. 1999. "Neurogenin1 and neurogenin2 Control Two Distinct Waves of Neurogenesis in Developing Dorsal Root Ganglia." *Genes & Development* 13, no. 13: 1717–1728.
- Marco, E. J., L. B. Hinkley, S. S. Hill, and S. S. Nagarajan. 2011. "Sensory Processing in Autism: A Review of Neurophysiologic Findings." *Pediatric Research* 69, no. 5: 48R–54R.
- Marmigere, F., and P. Ernfors. 2007. "Specification and Connectivity of Neuronal Subtypes in the Sensory Lineage." *Nature Reviews. Neuroscience* 8, no. 2: 114–127.
- McChesney, N., J. L. Barth, J. A. Rumschlag, et al. 2022. "Peripheral Auditory Nerve Impairment in a Mouse Model of Syndromic Autism." *Journal of Neuroscience* 42, no. 42: 8002–8018.
- Meltzer, S., C. Santiago, N. Sharma, and D. D. Ginty. 2021. "The Cellular and Molecular Basis of Somatosensory Neuron Development." *Neuron* 109, no. 23: 3736–3757.
- Mighell, T. L., S. Evans-Dutson, and B. J. O'Roak. 2018. "A Saturation Mutagenesis Approach to Understanding PTEN Lipid Phosphatase Activity and Genotype-Phenotype Relationships." *American Journal of Human Genetics* 102, no. 5: 943–955.
- Monday, H. R., H. C. Wang, and D. E. Feldman. 2023. "Circuit-Level Theories for Sensory Dysfunction in Autism: Convergence Across Mouse Models." *Frontiers in Neurology* 14: 1254297.
- Nolan, S. O., T. S. Jefferson, C. D. Reynolds, et al. 2019. "Neuronal Deletion of Phosphatase and Tensin Homolog Results in Cerebellar Motor Learning Dysfunction and Alterations in Intracellular Signaling." *Neuroreport* 30, no. 8: 556–561.
- Oliver, K. M., D. M. Florez-Paz, T. C. Badea, G. Z. Mentis, V. Menon, and J. C. de Nooij. 2021. "Molecular Correlates of Muscle Spindle and Golgi Tendon Organ Afferents." *Nature Communications* 12, no. 1: 1451.
- Orefice, L. L., J. R. Mosko, D. T. Morency, et al. 2019. "Targeting Peripheral Somatosensory Neurons to Improve Tactile-Related Phenotypes in ASD Models." *Cell* 178, no. 4: 867–886.
- Orefice, L. L., A. L. Zimmerman, A. M. Chirila, S. J. Sleboda, J. P. Head, and D. D. Ginty. 2016. "Peripheral Mechanosensory Neuron Dysfunction Underlies Tactile and Behavioral Deficits in Mouse Models of ASDs." *Cell* 166, no. 2: 299–313.
- Patel, T. D., A. Jackman, F. L. Rice, J. Kucera, and W. D. Snider. 2000. "Development of Sensory Neurons in the Absence of NGF/TrkA Signaling In Vivo." *Neuron* 25, no. 2: 345–357.
- Philpott, K. L., M. J. McCarthy, A. Klippel, and L. L. Rubin. 1997. "Activated Phosphatidylinositol 3-Kinase and Akt Kinase Promote Survival of Superior Cervical Neurons." *Journal of Cell Biology* 139, no. 3: 809–815.
- Pomaville, M. B., and K. M. Wright. 2023. "Follicle-Innervating Adelta-Low Threshold Mechanoreceptive Neurons Form Receptive Fields Through Homotypic Competition." *Neural Development* 18, no. 1: 2.
- Postigo, A., A. M. Calella, B. Fritzsch, et al. 2002. "Distinct Requirements for TrkB and TrkC Signaling in Target Innervation by Sensory Neurons." *Genes & Development* 16, no. 5: 633–645.
- Price, T. J., and O. K. Melemedjian. 2012. "Fragile X Mental Retardation Protein (FMRP) and the Spinal Sensory System." *Results and Problems in Cell Differentiation* 54: 41–59.

- Qi, L., M. Iskols, D. Shi, et al. 2024. "A Mouse DRG Genetic Toolkit Reveals Morphological and Physiological Diversity of Somatosensory Neuron Subtypes." *Cell* 187, no. 6: 1508–1526.
- Reichardt, L. F. 2006. "Neurotrophin-Regulated Signalling Pathways." *Philosophical Transactions of the Royal Society of London. Series B, Biological Sciences* 361, no. 1473: 1545–1564.
- Rutlin, M., C. Y. Ho, V. E. Abraira, et al. 2014. "The Cellular and Molecular Basis of Direction Selectivity of Adelta-LTMRs." *Cell* 159, no. 7: 1640–1651.
- Sarn, N., S. Thacker, H. Lee, and C. Eng. 2021. "Germline Nuclear-Predominant Pten Murine Model Exhibits Impaired Social and Perseverative Behavior, Microglial Activation, and Increased Oxytocinergic Activity." *Molecular Autism* 12, no. 1:41.
- Seal, R. P., X. Wang, Y. Guan, et al. 2009. "Injury-Induced Mechanical Hypersensitivity Requires C-Low Threshold Mechanoreceptors." *Nature* 462, no. 7273: 651–655.
- Sharma, N., K. Flaherty, K. Lezgiyeva, D. E. Wagner, A. M. Klein, and D. D. Ginty. 2020. "The Emergence of Transcriptional Identity in Somatosensory Neurons." *Nature* 577, no. 7790: 392–398.
- Skelton, P. D., R. V. Stan, and B. W. Luikart. 2020. "The Role of PTEN in Neurodevelopment." *Molecular Neuropsychiatry* 5, no. 1: 60–71.
- Snider, W. D. 1994. "Functions of the Neurotrophins During Nervous System Development: What the Knockouts Are Teaching Us." *Cell* 77, no. 5: 627–638.
- Snider, W. D., and I. Silos-Santiago. 1996. "Dorsal Root Ganglion Neurons Require Functional Neurotrophin Receptors for Survival During Development." *Philosophical Transactions of the Royal Society of London. Series B, Biological Sciences* 351, no. 1338: 395–403.
- Song, W., M. Volosin, A. B. Cragnolini, B. L. Hempstead, and W. J. Friedman. 2010. "ProNGF Induces PTEN via p75NTR to Suppress Trk-Mediated Survival Signaling in Brain Neurons." *Journal of Neuroscience* 30, no. 46: 15608–15615.
- Suzuki, A., J. L. de la Pompa, V. Stambolic, et al. 1998. "High Cancer Susceptibility and Embryonic Lethality Associated With Mutation of the PTEN Tumor Suppressor Gene in Mice." *Current Biology* 8, no. 21: 1169–1178.
- Tasnim, A., I. Alkislar, R. Hakim, et al. 2024. "The Developmental Timing of Spinal Touch Processing Alterations Predicts Behavioral Changes in Genetic Mouse Models of Autism Spectrum Disorders." *Nature Neuroscience* 27, no. 3: 484–496.
- Tilot, A. K., T. W. Frazier 2nd, and C. Eng. 2015. "Balancing Proliferation and Connectivity in PTEN-Associated Autism Spectrum Disorder." *Neurotherapeutics* 12, no. 3: 609–619.
- Tomchek, S. D., and W. Dunn. 2007. "Sensory Processing in Children With and Without Autism: A Comparative Study Using the Short Sensory Profile." *American Journal of Occupational Therapy* 61, no. 2: 190–200.
- Uljarevic, M., T. W. Frazier, G. Rached, et al. 2021. "Toward Better Characterization of Restricted and Repetitive Behaviors in Individuals With Germline Heterozygous PTEN Mutations." *American Journal of Medical Genetics. Part A* 185, no. 11: 3401–3410.
- Usoskin, D., A. Furlan, S. Islam, et al. 2015. "Unbiased Classification of Sensory Neuron Types by Large-Scale Single-Cell RNA Sequencing." *Nature Neuroscience* 18, no. 1: 145–153.
- Vlasits, A. L., M. Syeda, A. Wickman, et al. 2025. "Atypical Retinal Function in a Mouse Model of Fragile X Syndrome." *Journal of Neuroscience* 45, no. 27: 1–13.
- Worby, C. A., and J. E. Dixon. 2014. "PTEN." Annual Review of Biochemistry 83: 641-669.
- Yehia, L., and C. Eng. 2018. "65 Years of the Double Helix: One Gene, Many Endocrine and Metabolic Syndromes: PTEN-Opathies and Precision Medicine." *Endocrine-Related Cancer* 25, no. 8: T121–T140.

Yehia, L., E. Keel, and C. Eng. 2020. "The Clinical Spectrum of PTEN Mutations." *Annual Review of Medicine* 71: 103–116.

Yeung, K. S., W. W. Y. Tso, J. J. K. Ip, et al. 2017. "Identification of Mutations in the PI3K-AKT-mTOR Signalling Pathway in Patients With Macrocephaly and Developmental Delay and/or Autism." *Molecular Autism* 8: 66.

York, R. D., D. C. Molliver, S. S. Grewal, P. E. Stenberg, E. W. McCleskey, and P. J. S. Stork. 2000. "Role of Phosphoinositide 3-Kinase and Endocytosis in Nerve Growth Factor-Induced Extracellular Signal-Regulated Kinase Activation via Ras and Rap1." *Molecular and Cellular Biology* 20, no. 21: 8069–8083.

Zhang, D., J. Turecek, S. Choi, et al. 2024. "C-LTMRs Evoke Wet Dog Shakes via the Spinoparabrachial Pathway." *Science* 386, no. 6722: 686–692.

Zheng, Y., P. Liu, L. Bai, J. S. Trimmer, B. P. Bean, and D. D. Ginty. 2019. "Deep Sequencing of Somatosensory Neurons Reveals Molecular Determinants of Intrinsic Physiological Properties." *Neuron* 103, no. 4: 598–616

Zimmerman, A. L., E. M. Kovatsis, R. Y. Pozsgai, A. Tasnim, Q. Zhang, and D. D. Ginty. 2019. "Distinct Modes of Presynaptic Inhibition of Cutaneous Afferents and Their Functions in Behavior." *Neuron* 102, no. 2: 420–434.

Zylka, M. J., F. L. Rice, and D. J. Anderson. 2005. "Topographically Distinct Epidermal Nociceptive Circuits Revealed by Axonal Tracers Targeted to Mrgprd." *Neuron* 45, no. 1: 17–25.

#### **Supporting Information**

Additional supporting information can be found online in the Supporting Information section. Figure S1: Co-expression of subtypespecific markers suggests specification phenotypes in PtenHet mutants. (A) Representative images (left) and quantification (right) of TrkA (green) and CGRP (magenta) co-immunolabeling in cryosections of adult DRGs in WT and PtenHet mice showing equal proportions of double-labeled neurons  $(0.96 \pm 0.01 \text{ in WT vs. } 0.97 \pm 0.02 \text{ in } Pten^{Het}$ , n=5, p=0.91, Wilcoxon rank sum test). (B) Representative images (left) and quantification (right) of Th (green) and kv4.3 (magenta) immunolabeling in WT and PtenHet mice showing equal proportions of double-labeled neurons  $(1.01 \pm 0.02 \text{ in WT vs. } 1.03 \pm 0.04 \text{ in } Pten^{Het}$ , n=5, p=0.834, Wilcoxon rank sum test). (C) Images (left) and quantification (right) of immunostaining of TrkC (green) and Etv1 (magenta) showing no significant differences in co-labeled populations in mutants compared to controls  $(0.96 \pm 0.007 \text{ in WT vs. } 0.97 \pm 0.02 \text{ in } Pten^{Het}, n = 5,$ p = 0.91, Wilcoxon rank sum test). **Figure S2:** Proliferation and developmental cell death are normal in *Pten*<sup>Het</sup> mutants. (A) Representative images of E11.5 DRGs from WT and PtenHet littermates birth-dated with EdU and labeled with Sox10 immunostaining (left panels) (Scale 100 μm). Quantification (right panel) shows the percentage of Sox10+ progenitors undergoing proliferation at each developmental time point (E9.5-E14.5). At all ages quantified, there is no significant difference in the percentage of EdU+; Sox10+ precursors in PtenHet compared to WT controls (n = 5, E9.5-E14.5: p > 0.5 for each timepoint, 2-way ANOVA followed by Tukey's HSD post hoc pair-wise comparisons with correction for multiple testing). (B) Representative images from E11.5 DRGs of WT and PtenHet littermates showing activated Caspase 3 (Casp3; green) and Islet 1/2 immunoreactivity (left panels) (Scale 100 µm). Quantification (right panel) shows the percentage of Isl1/2+ neurons co-labeled with activated Caspase 3. At all ages quantified (E10.5- E14.5), there is no significant difference in the percentage of activated Casp3+; Islet1+ neurons in  $Pten^{Het}$  DRGs compared to WT controls (n = 5, E9.5-E14.5: p > 0.1for each timepoint, 2-way ANOVA followed by Tukey's HSD post hoc pair-wise comparisons with correction for multiple testing). Table S1: Differentially expressed genes between wildtype and PtenHet mutant dorsal root ganglia neurons.